

Scripta Materialia

Achieving Excellent Strength-Toughness Combination in Hexagonal Closed-Packed Multi-Principle Element Alloys via $\langle c+a \rangle$ Slip Promotion

--Manuscript Draft--

Manuscript Number:	SMM-23-1224R1
Article Type:	Regular article
Keywords:	hexagonal-close packed structure; multi-principle element alloys; dislocation plasticity; generalized stacking fault energy; strength-toughness combination
Corresponding Author:	Jie Kuang, Ph.D. Xi'an Jiaotong University CHINA
First Author:	Jie Kuang, Ph.D.
Order of Authors:	Jie Kuang, Ph.D. Dongdong Zhang, PhD Yuqing Zhang Xinpeng Du, PhD Qinghuan Huo, PhD Wei Wen, PhD Fuyang Tian, PhD Gang Liu, PhD Jinyu Zhang, PhD Jun Sun, PhD
Abstract:	<p>To effectively bolster $\langle c+a \rangle$ slip is pivotal to improving the mechanical property of hexagonal close-packed (HCP) metallic materials. It has been a longstanding challenge facing the structural material community. Here we introduce a strategy to crack this hard nut. Employing two coarse-grained Ti-Zr-Hf model alloys as examples, we demonstrate for the first time that the two intrinsic properties of multi-principle element alloys (MPEAs)—high alloy concentration and local fluctuation—can work synergistically to narrow the gap in nucleation/gliding resistance between non-prismatic slip and prismatic slip, leading to enhanced activities of $\langle c+a \rangle$ and first order pyramidal $\langle a \rangle$ dislocations. This renders the material an exceptional strength-toughness combination, outperforming other coarse-grained HCP alloys and even rivalling most of those with delicately designed microstructures including nanostructures and heterostructures. Given the high concentration and local fluctuation are intrinsic to all MPEAs, we anticipate that this strategy could extend to other MPEAs featuring an HCP structure.</p>



西安交通大学
XI'AN JIAOTONG UNIVERSITY

State Key Lab for Mechanical behavior of Materials

Nov. 7, 2023

Prof. Lei Lu

Editor

Scripta Materialia

RE: Ms. No. SMM-23-1224, “Achieving Excellent Strength-Toughness Combination in Hexagonal Closed-Packed Multi-Principle Element Alloys via $\langle c+a \rangle$ Slip Promotion” by J. Kuang, D. Zhang, Y. Zhang, X. Du, Q. Huo, W. Wen, F. Tian, G. Liu, J. Zhang, and J. Sun

Dear Prof. Lu,

Thank you for your note on October 9th, indicating a willingness to reevaluate our revised submission for potential publication.

We have meticulously reviewed the feedback provided by the reviewers, conducted additional experiments and simulations, and substantially revised our manuscript and supplementary materials. Key updates have been marked in yellow for ease of identification. We have also included a detailed response to the reviewers' comments with our submission.

We believe these enhancements have greatly improved the paper, and we hope it now meets the journal's standards for publication.

We are grateful for your attention to our work.

Sincerely,

Gang Liu, PhD

Professor

State Key Lab for Mechanical Behavior of Materials

Xi'an Jiaotong University

Gang Liu

Professor of Materials Science and Engineering
Vice director - State Key Lab for Mechanical Behavior of Materials

Cyrus Tang Building, 28 Xianning West Road
Xi'an 710049, P.R. China

Tel: +86 29 8266 8614 Fax: +86 29 8266 8614

Email: lgsammer@xjtu.edu.cn

Response to Reviewers

Ms. Ref. No.: SMM-23-1224

"Achieving Excellent Strength-Toughness Combination in Hexagonal Closed-Packed Multi-Principle Element Alloys via $\langle c+a \rangle$ Slip Promotion" by J. Kuang, D. Zhang, Y. Zhang, X. Du, Q. Huo, W. Wen, F. Tian, G. Liu, J. Zhang, J. Sun

Reviewer #1:

The paper titled "Achieving Excellent Strength-Toughness Combination in Hexagonal Closed-Packed Multi-Principle Element Alloys via Slip Promotion" by Kuang et al. have presented a detailed study of MPEAs with an exceptional strength-toughness combination by both experiments and first-principle calculations. The high concentration and local fluctuation are confirmed to be the keys in the high strength-toughness combination-MPEAs in this work. However, some papers have also mentioned the effect of extent of solute and local fluctuation [1] on strength-ductility in Ti and other alloys, and this does not provide a new perspective for designing high strength-toughness MPEAs alloys. This is well written paper but this manuscript lacks of novelty and hardly satisfy the aims/scopes of Scripta Materialia. Some detailed comments that could be suggested to improve it are listed below.

Response: We appreciate the reviewer's insights on this matter. The authors fully agree with the reviewer's statement that there are some publication in recent years on the topic of solute fluctuation and how it affects the dislocation activity and mechanical properties. However, upon reviewing these studies, we observed that their focus predominantly lies on FCC or BCC metals/alloys [1-8], including the one kindly provided by the reviewer, which is on FCC CoCrFeMnNi [1]. To the best of our knowledge, there is not much investigation into materials with a single-phase HCP structure [2, 3, 9], where the dislocation plasticity is more complicated than cubic materials: the mechanical response is affected not only by a single slip mode (for example, the $\{111\} \langle 1\bar{1}0 \rangle$ slip mode in FCC) but also by the **relative nucleation/gliding resistance of different slip modes**. Consequently, while the influence of local fluctuation on strengthening is acknowledged, the specific effects it

might have on the **different slip modes in HCP alloys**, especially pertaining to the **relative nucleation/gliding resistance**, remain an open question. This is the reason why the authors feel it is necessary to perform the present work. For the reviewer's reference, the authors list here two novel perspectives that our study brings to the table for the HCP structural material community:

- 1) This work shows **for the first time** that the relative ease of different slip modes (basal<a>, Prism<a>, Pyr1<a>, Pyr1<c+a>, Pyr2<c+a> etc.) in HCP alloys can be affected/tailored by the solute fluctuation;
- 2) The Ti-Zr-Hf model alloys, despite their **coarse-grained structure**, exhibit an exceptional combination of strength and toughness. They not only **surpass all existing single-phase coarse-grained HCP alloys** but also **rival most of those bearing meticulously designed microstructures**. Building on this foundation, we expect that by integrating our current approach with traditional strengthening techniques, even more superior mechanical properties can be obtained.

The authors feel the contribution in this work is timely yet novel to further stimulate the field of MPEAs towards tackling the age-old issue of the wide activation/gliding resistance gap among the soft and hard slip modes in HCP materials. We trust that these points adequately address the concerns raised about the manuscript's novelty and thank the reviewer for prompting this clarification.

Reference

- [1] Utt, D., Lee, S., Xing, Y., Jeong, H., Stukowski, A., Oh, S.H., Dehm, G. and Albe, K., 2022. The origin of jerky dislocation motion in high-entropy alloys. *Nature communications*, 13(1), p.4777.
- [2] Ma, E., 2020. Unusual dislocation behavior in high-entropy alloys. *Scripta Materialia*, 181, pp.127-133.
- [3] Basu, I. and De Hosson, J.T.M., 2020. Strengthening mechanisms in high entropy alloys: fundamental issues. *Scripta Materialia*, 187, pp.148-156.
- [4] Wang, L., Ding, J., Chen, S., Jin, K., Zhang, Q., Cui, J., Wang, B., Chen, B., Li, T., Ren, Y. and Zheng, S., 2023. Tailoring planar slip to achieve pure metal-like ductility in body-centred-cubic multi-principal element alloys. *Nature Materials*, pp.1-8.
- [5] Smith, L.T., Su, Y., Xu, S., Hunter, A. and Beyerlein, I.J., 2020. The effect of local chemical ordering on Frank-Read source activation in a refractory multi-principal element alloy. *International*

Journal of Plasticity, 134, p.102850.

[6] Wang, F., Balbus, G.H., Xu, S., Su, Y., Shin, J., Rottmann, P.F., Knipling, K.E., Stinville, J.C., Mills, L.H., Senkov, O.N. and Beyerlein, I.J., 2020. Multiplicity of dislocation pathways in a refractory multiprincipal element alloy. *Science*, 370(6512), pp.95-101.

[7] Li, Q.J., Sheng, H. and Ma, E., 2019. Strengthening in multi-principal element alloys with local-chemical-order roughened dislocation pathways. *Nature communications*, 10(1), p.3563.

[8] Ding, Q., Zhang, Y., Chen, X., Fu, X., Chen, D., Chen, S., Gu, L., Wei, F., Bei, H., Gao, Y. and Wen, M., 2019. Tuning element distribution, structure and properties by composition in high-entropy alloys. *Nature*, 574(7777), pp.223-227.

[9] Gao, M.C., Zhang, B., Guo, S.M., Qiao, J.W. and Hawk, J.A., 2016. High-entropy alloys in hexagonal close-packed structure. *Metallurgical and Materials Transactions A*, 47, pp.3322-3332.

1. Page 2, Line 37-40: Many works [2,3] have reported that the increasing absolute CRSS values for pyramidal slip systems by alloying atoms in HCP alloys, such as Mg alloys, Ti alloys and Zn alloys.

Response: Apologies for the confusion. Indeed, as noted by the reviewer, numerous solute elements, notably most rare-earth elements, can enhance the absolute CRSS values for pyramidal slip systems. In the previous version of our manuscript, we stated “Moreover, **in many cases**, while solute additions do improve $\langle c+a \rangle$ activity, they decrease not only the activation/gliding resistance anisotropy among different slip modes but also the absolute values of the activation/gliding resistance of the hard deformation modes”. Our intention was to highlight a worst-case scenario. It did not mean to suggest that all solute atoms inevitably lead to a reduction in the absolute CRSS values for pyramidal slip.

In light of the reviewer’s feedback, we have revised our wording to specify “in some extreme cases” instead of “in many cases” to eliminate any potential misunderstanding. In addition, we have added some representative references (including the two provided by the reviewer) in case any readers are interested in more detailed discussions on this topic. We are thankful for the reviewer’s attentive reading and constructive feedback, which have greatly assisted in clarifying this point.

2. It was mentioned that the slip traces in MPEAs are thinner and denser compared to those in pure Ti, highlighting the different deformation homogeneity in the two material categories. It was quite confused to say "thinner and denser". The localized deformation with localized slip traces means inhomogeneous deformation.

Response: We appreciate the reviewer's attention to detail and for highlighting this language issue. Using h to symbolize the height of a slip step in slip trace analysis, we can express h as $h = n \cdot |\vec{b}|$, where n denotes the number of dislocations leaving the surface and \vec{b} the Burgers vector. When h has smaller values, signifying finer slip traces, it suggests fewer dislocations involved in each slip trace. An increased or denser number of slip lines aligns with more spread-out deformation (in meso scale). The text is now reworded to make the argument clear.

"Surface morphology observations reveal that the slip traces in MPEAs are finer and more abundant compared to those in pure Ti. Considering the $h = n \cdot |\vec{b}|$ relation (where h denotes the height of the slip step, n the number of dislocations leaving the surface, and \vec{b} the Burgers vector), this observation indicates a less concentrated and more spread-out deformation (in mesoscale) in the MPEAs with lower individual shear strain borne by each slip plane."

3. Page 11, Line 3-8: There is the sentence of "As Pyr2 slip traces can be produced by slip systems no other than $\{11\bar{2}2\} \langle 11\bar{2}3 \rangle$ (Pyr2), the denser Pyr2 slip traces in T1.2 and T1.0 indicate higher Pyr2 activities in the two MPEAs compared to pure Ti". The authors emphasized the Pyr2 slip traces can be generated by other slip systems, but then they mentioned that the Pyr2 traces in T1.2/T1.0 were higher than that in Ti. Please check the orientation of slip traces in different alloying systems in this work by other methods of characterization (such as TEM). Meanwhile, the mean-free-path of dislocations are much shorter than dislocations [4]. Thus, it is possible that the slip traces of dislocations cannot be observed on the surface of the sample.

Response:

1) Regarding the interpretation of Pyr2 slip traces:

As pointed out by the reviewer, we in fact stated “As Pyr2 slip traces can be produced by slip systems **NO OTHER THAN** $\{11\bar{2}2\} \langle 11\bar{2}3 \rangle$ (Pyr2), the denser Pyr2 slip traces in T1.2 and T1.0 indicate higher Pyr2 activities in the two MPEAs compared to pure Ti”. By saying this, we meant to emphasize that the observed Pyr2 slip traces can ONLY be attributed to Pyr2 $\langle c+a \rangle$ slip. The increased frequency of these traces in T1.2 and T1.0, compared to pure Ti, led us to conclude a higher activity of Pyr2 $\langle c+a \rangle$ slip in the MPEAs. This methodology (using Pyr2 slip trace as an indicator of Pyr2 $\langle c+a \rangle$ slip) aligns with several other published studies [1-8].

However, in light of the reviewer’s feedback, we took the initiative to rephrase the statements in question in the revised manuscript to prevent any potential misunderstanding. We believe that this adjustment will contribute to a clearer and more straightforward presentation of our findings. Here is the revised sentence for the reviewer’s reference:

“As Pyr2 slip traces can be only produced by slip system $\{11\bar{2}2\} \langle 11\bar{2}3 \rangle$ (Pyr2), the more profuse Pyr2 slip traces in T1.2 and T1.0 indicate higher Pyr2 $\langle c+a \rangle$ activities in the MPEAs compared to pure Ti.”

2) Regarding the dislocation mean-free-path and the shortcomings of the SEM slip trace observation:

The reviewer brings up a very important point. Indeed, we concur that the extracted data from SEM slip trace analysis is, strictly speaking, an underestimation since it only account for the dislocations that escape the sample surface. There could be significant dislocation-dislocation interactions in the interior of the sample, such that sessile segments and dislocation sources are generated and remain within the bulk.

Therefore, in alignment with the reviewer's recommendation, we extended our investigation to include TEM-based Burgers vector and slip trace analysis at a true plastic strain of ~ 0.08 (the same strain as in the SEM slip trace analysis shown in Fig. 2), aiming to uncover any unique dislocation modes potentially overlooked by the SEM

method. Unfortunately, the elevated dislocation density ($7\sim 11 \times 10^{14} \text{ m}^{-2}$ by CMWP) and entanglements prevented us from extracting reliable data. This is actually a long-time technical challenge facing researchers in the field of HCP materials such as Mg, and why TEM Burgers vector and slip trace analysis are often performed at strains lower than 0.05 [9-15]. Considering the scope of our study is focused on a semi-quantitative, or even qualitative, comparative analysis of slip activities across different materials, we maintain that the SEM slip trace analysis, as endorsed by numerous researchers [1-8], remains a viable method. This assertion holds especially true when one considers that the method yields extensive and reliable statistical data, and in our study, is even further validated by the incorporation of TEM ($\epsilon_p = 0.02$) and CMWP analyses. **In the revised manuscript sentences have been added to remind the readers about the shortcomings of the SEM based slip trace analysis.**

Reference

- [1] Du, C., Gao, Y., Hua, Z.M., Zha, M., Wang, C. and Wang, H.Y., 2022. Enhanced superplasticity achieved by disclination-dislocation reactions in a fine-grained low-alloyed magnesium system. *International Journal of Plasticity*, 154, p.103300.
- [2] Lunt, D., Thomas, R., Atkinson, M.D., Smith, A., Sandala, R., da Fonseca, J.Q. and Preuss, M., 2021. Understanding the role of local texture variation on slip activity in a two-phase titanium alloy. *Acta Materialia*, 216, p.117111.
- [3] Bian, M., Huang, X. and Chino, Y., 2021. Substantial improvement in cold formability of concentrated Mg–Al–Zn–Ca alloy sheets by high temperature final rolling. *Acta Materialia*, 220, p.117328.
- [4] Zhu, G., Wang, L., Zhou, H., Wang, J., Shen, Y., Tu, P., Zhu, H., Liu, W., Jin, P. and Zeng, X., 2019. Improving ductility of a Mg alloy via non-basal $\langle a \rangle$ slip induced by Ca addition. *International Journal of Plasticity*, 120, pp.164-179.
- [5] Shi, D.F., Pérez-Prado, M.T. and Cepeda-Jiménez, C.M., 2019. Effect of solutes on strength and ductility of Mg alloys. *Acta Materialia*, 180, pp.218-230.
- [6] Zeng, Z.R., Bian, M.Z., Xu, S.W., Davies, C.H.J., Birbilis, N. and Nie, J.F., 2016. Effects of dilute additions of Zn and Ca on ductility of magnesium alloy sheet. *Materials Science and Engineering: A*, 674, pp.459-471.
- [7] Boehlert, C.J., Chen, Z., Gutiérrez-Urrutia, I., Llorca, J. and Pérez-Prado, M.T., 2012. In situ analysis of the tensile and tensile-creep deformation mechanisms in rolled AZ31. *Acta Materialia*, 60(4), pp.1889-1904.
- [8] Molodov, K.D., Al-Samman, T. and Molodov, D.A., 2017. Profuse slip transmission across twin boundaries in magnesium. *Acta Materialia*, 124, pp.397-409.
- [9] Agnew, S.R., Horton, J.A. and Yoo, M.H., 2002. Transmission electron microscopy investigation of $\langle c+a \rangle$ dislocations in Mg and α -solid solution Mg-Li alloys. *Metallurgical and*

Materials Transactions A, 33, pp.851-858.

[10] Chong, Y., Gholizadeh, R., Tsuru, T., Zhang, R., Inoue, K., Gao, W., Godfrey, A., Mitsuhashi, M., Morris Jr, J.W., Minor, A.M. and Tsuji, N., 2023. Grain refinement in titanium prevents low temperature oxygen embrittlement. Nature communications, 14(1), p.404.

[11] Koike, J., Kobayashi, T., Mukai, T., Watanabe, H., Suzuki, M., Maruyama, K. and Higashi, K., 2003. The activity of non-basal slip systems and dynamic recovery at room temperature in fine-grained AZ31B magnesium alloys. Acta materialia, 51(7), pp.2055-2065.

[12] Wei, K., Hu, R., Yin, D., Xiao, L., Pang, S., Cao, Y., Zhou, H., Zhao, Y. and Zhu, Y., 2021. Grain size effect on tensile properties and slip systems of pure magnesium. Acta Materialia, 206, p.116604.

[13] Zhao, D., Ma, X., Picak, S., Karaman, I. and Xie, K., 2020. Activation and suppression of $\langle c+a \rangle$ dislocations in a textured Mg–3Al–1Zn alloy. Scripta Materialia, 179, pp.49-54.

[14] Wu, Z., Ahmad, R., Yin, B., Sandlőbes, S. and Curtin, W.A., 2018. Mechanistic origin and prediction of enhanced ductility in magnesium alloys. Science, 359(6374), pp.447-452.

[15] Sandlőbes, S., Pei, Z., Friők, M., Zhu, L.F., Wang, F., Zaefferer, S., Raabe, D. and Neugebauer, J., 2014. Ductility improvement of Mg alloys by solid solution: Ab initio modeling, synthesis and mechanical properties. Acta Materialia, 70, pp.92-104.

4. The DFT calculation is used to get the GSFE in pure Ti and Ti1.2 alloy. It is hard to consider alloy concentration from the view point of DFT calculation. And how to distinguish Ti1.0 and Ti1.2 alloy?

Response:

1) Regarding the consideration of alloy concentration using DFT:

DFT has been frequently employed in literature to study the influence of (micro-)alloying on the GSFE of conventional alloys [1-3]. Standard DFT calculations on materials typically rely on crystalline structures with ordered atomic arrangements and specific stoichiometry. For pure Ti, we employed this standard approach. For multi-principal element alloys, however, the situation becomes more intricate. In order to treat the chemical disorder, two commonly used approaches have been proposed in the literature. The first is the mean field based coherent potential approach [4] or virtual lattice approximation, which can treat any concentration in alloys, but ignore the effect of local atomic environment in alloys. The second is the supercell method [5], in which the size of supercell strongly depends on the alloy concentration. In this method, the chemical disorder is simulated via the quasi-random similar atomic environment or clusters (pair-atom cluster and three-atom cluster) with the optimized objective function

[5, 6]. One co-author of the present work recently introduced the similar atomic environment (SAE) approach for structural modeling of solid-solution materials [7]. This method provides a uniform way to take into account both full disorder and short range order (SRO) via minimizing the objective function in the configuration space, offering an effective approach to the study of phase stability, mechanical properties, and electronic structure for solid-solution materials. With its effectiveness being demonstrated across various materials [7-9], we utilized the SAE method in our present calculations of T1.2. For readers seeking a deeper dive into our DFT calculations, we have dedicated a subsection in the [Supplementary Materials](#) to elucidate the methodology.

2) Regarding distinguishing T1.0 and T1.2:

Our primary objective in this study is not to delineate the subtle differences in dislocation behaviors and mechanical properties between T1.0 and T1.2. Both MPEAs exhibit qualitatively similar behaviors. Our focus is directed towards highlighting the influences of high alloy concentration and solute fluctuation intrinsic to all MPEAs. This can be achieved by comparing either of the two MPEAs with pure Ti.

Initially, our manuscript was centered solely on T1.2 and pure Ti. The inclusion of T1.0 was a subsequent decision, aimed at emphasizing that the observed effects of high alloy concentration and solute fluctuation aren't specific to T1.2 but are broader phenomena at least for Ti-Zr-Hf systems. Given the congruent trends observed in both T1.0 and T1.2 (in comparison to pure Ti), we limited our DFT calculations to T1.2 and showcased it as a representative material to explore the implications of solute fluctuation on dislocation nucleation and gliding resistance.

We acknowledge the reviewer's suggestion to delve deeper into the difference between T1.0 and T1.2, and it is indeed a captivating aspect. However, given the computational intensity associated with GSFE calculations that incorporate solute fluctuations, we believe such an exhaustive analysis extends beyond the scope of this concise communication paper. Nevertheless, we are in the process of developing a multiscale crystal plasticity model that integrates the complexities of solute fluctuations

in MPEAs. This ongoing work involves calculating the GSFE curves for several Ti-Zr-Hf alloys, including T1.0, facilitating a derivation of the Peierls stress which is subsequently employed as an input in the CPFEM model. This enhanced model, coupled with the new GSFE data, is anticipated to offer illuminating insights into the distinctions in dislocation plasticity and mechanical properties across different Ti-Zr-Hf MPEAs.

We've reworded the revised manuscript to accentuate the qualitative similarities between T1.0 and T1.2 when compared with pure Ti. We hope this clarification delineates our rationale for selecting T1.2 as a representative example to elucidate the distinctions between the MPEAs and pure Ti.

Reference

- [1] Muzyk, M., Pakiel, Z.A. and Kurzydowski, K.J., 2012. Generalized stacking fault energy in magnesium alloys: Density functional theory calculations. *Scripta Materialia*, 66(5), pp.219-222.
- [2] Kale, C., Garg, P., Bazehour, B.G., Srinivasan, S., Bhatia, M.A., Peralta, P. and Solanki, K.N., 2019. Oxygen effects on crystal plasticity of Titanium: A multiscale calibration and validation framework. *Acta Materialia*, 176, pp.19-32.
- [3] Sun, H., Ding, Z., Zhang, D., Zhou, H., Li, S., Lavernia, E.J., Zhu, Y. and Liu, W., 2019. Predicting the formation of $\langle c+a \rangle$ dislocations in magnesium alloys from multiple stacking fault energies. *Materialia*, 7, p.100352.
- [4] Soven, P., 1967. Coherent-potential model of substitutional disordered alloys. *Physical Review*, 156(3), p.809.
- [5] Zunger, A., Wei, S.H., Ferreira, L.G. and Bernard, J.E., 1990. Special quasirandom structures. *Physical review letters*, 65(3), p.353.
- [6] Tian, F., 2017. A review of solid-solution models of high-entropy alloys based on ab initio calculations. *Frontiers in Materials*, 4, p.36.
- [7] Tian, F., Lin, D.Y., Gao, X., Zhao, Y.F. and Song, H.F., 2020. A structural modeling approach to solid solutions based on the similar atomic environment. *The Journal of chemical physics*, 153(3).
- [8] Wang, S.D., Liu, X.J., Lei, Z.F., Lin, D.Y., Bian, F.G., Yang, C.M., Jiao, M.Y., Du, Q., Wang, H., Wu, Y. and Jiang, S.H., 2021. Chemical short-range ordering and its strengthening effect in refractory high-entropy alloys. *Physical Review B*, 103(10), p.104107.
- [9] Dong, H., Chen, H., Zhang, B., Zhang, Y., Wang, Z., Zhou, X., Wang, W., Wang, H., Li, T., Yang, Z. and van der Zwaag, S., 2022. Revealing the influence of Mo addition on interphase precipitation in Ti-bearing low carbon steels. *Acta Materialia*, 223, p.117475.

5. In Figs.4(d) and 4(e), it is notably that the restoring forces of Pyr1 and Pyr2 are similar in pure Ti and T1.2, which indicates that the ability of nucleation of the two dislocations are similar. The nucleation of dislocation can be achieved by 11 basal

stacking fault at some extent, while this process produces a partial dislocation [5], which cannot cross-slip to other pyramidal planes. Meanwhile, Peierls stresses of Pyr1 are much lower than Pyr2 in both pure Ti and T1.2, which means that the ability of full dislocations gliding on Pyr1 is easier than that on the Pyr2 planes. This is corresponding to a large difference between the gliding barrier of dislocations on Pyr1 and Pyr2 planes and hence, the cross-slips of dislocations are hard to achieve.

Response: We thank the reviewer for this comment. We concur with the reviewer's assessment regarding the comparable ease of nucleation for $\text{Pyr1}\langle c+a \rangle$ and $\text{Pyr2}\langle c+a \rangle$. As with the cross slip of $\langle c+a \rangle$ dislocations, our thoughts are as follows.

1) Regarding the relation between I_1 stacking fault and the possibility of cross slip:

The authors believe that while the I_1 basal stacking faults themselves cannot cross slip, the $\langle c+a \rangle$ dislocations generated by them are capable of doing so. Indeed, the $\langle c+a \rangle$ cross-slip among different pyramidal planes is well-documented, supported by both TEM observations and computational simulations [1-6]. Actually, right within the paper that was cited by the reviewer [1], which first proposed the I_1 stacking fault nucleation mechanism, we can find the occurrence of $\langle c+a \rangle$ cross slip between different pyramidal planes. In Fig. R1. [4] (the original data was first published by Sandlöbes on Acta Materialia [1]), we can see very clearly that there is high-frequency $\langle c+a \rangle$ cross slip between Pyr1 and Pyr2. The generation of the $\langle c+a \rangle$ dislocations from an I_1 stacking fault has been elaborated by Agnew et al. [6] and Basu et al. [7]. As shown in Fig. R2, the screw segment in (c) is capable of cross slip.

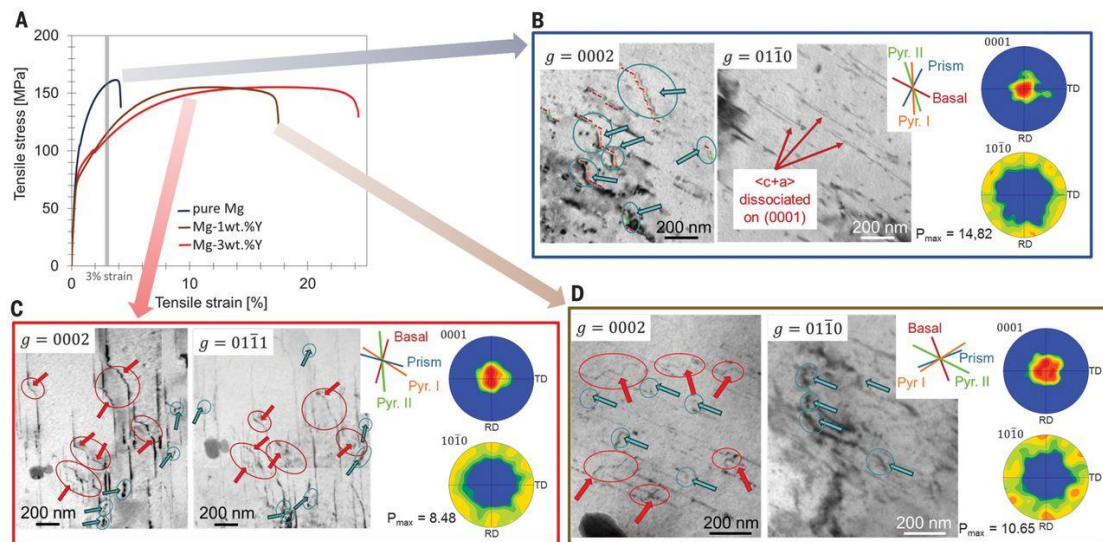


Fig. R1 Experimental results for pure Mg and Mg-Y alloys under tensile deformation at room temperature: (A) Stress-strain curves and (B to D) initial $\{0001\}$ and $\{10\bar{1}0\}$ pole figures and bright-field TEM of the corresponding dislocation microstructures after 2.5 to 3% strain for pure Mg (B), Mg-3 wt % Y (C), and Mg-1 wt % Y (D). In (B) to (D), dislocations visible under diffraction vector $g = 0002$ are $\langle c+a \rangle$ dislocations based on two-beam $g \cdot b = 0$ visibility analysis (b , Burgers vector); the insets show the corresponding crystallographic plane traces identified using diffraction analysis, enabling determination of the crystal planes of the observed $\langle c+a \rangle$ dislocations. In (B), $\langle c+a \rangle$ dislocation segments are lying on basal and pyramidal II planes; areas where dislocations change from pyramidal II to basal planes are highlighted by turquoise arrows and circles. In (C) and (D), $\langle c+a \rangle$ dislocation segments are predominantly on pyramidal II planes, with frequent plane changes to either pyramidal I (highlighted by red arrows and circles) or basal (highlighted by turquoise arrows and circles) planes. In (C), for Mg-3 wt % Y, high-frequency $\langle c+a \rangle$ dislocation switching between pyramidal II and I planes (double cross-slip) is evident. **The figure and caption are from Wu et al. [4]**

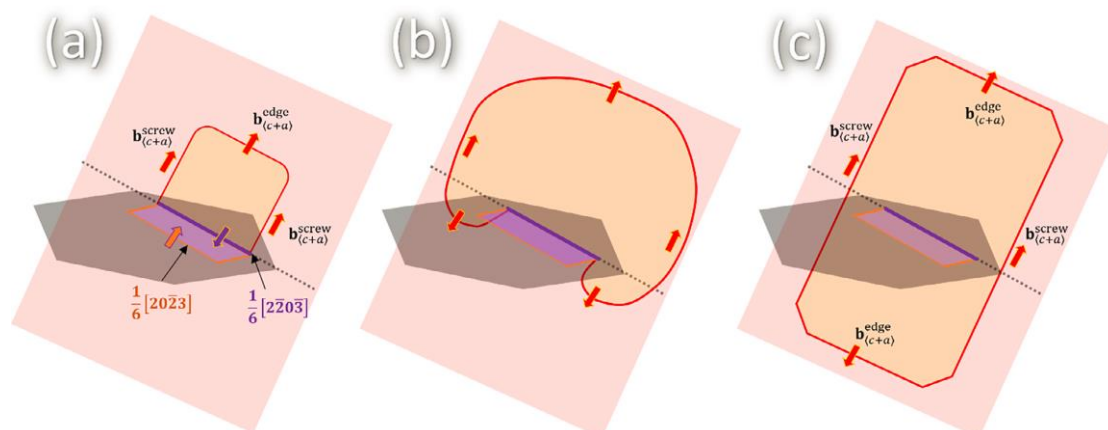


Fig. R2 Detailed schematic of $\langle c+a \rangle$ slip generation from I_1 stacking faults **The figure and caption are copied from Basu et al. [7]**

2) Regarding the Peierls stress difference between $\text{Pyr1}\langle c+a \rangle$ and $\text{Pyr2}\langle c+a \rangle$ and the cross slip

We agree with the reviewer that the Peierls stress of $\text{Pyr1}\langle c+a \rangle$ is much lower than that of $\text{Pyr2}\langle c+a \rangle$. This implies, as underscored by the reviewer, an easier glide of $\langle c+a \rangle$ dislocations on Pyr1 compared to Pyr2 . However, this does not necessarily mean that the $\langle c+a \rangle$ slip occurs on Pyr1 only. In fact, as substantiated by the experimentally observed Pyr2 slip trace displayed in Fig. 2, there is $\text{Pyr2}\langle c+a \rangle$ activity within the material. We believe this can be rationalized from the following several perspectives:

- a) In Fig. 4(d), the results show that the solute fluctuation (for example, $\sigma = 0.1$) significantly reduces the gap between the Pyr1 and Pyr2 . There is even an overlap region in the Peierls stress ratio for $\text{Pyr1}\langle c+a \rangle$ and $\text{Pyr2}\langle c+a \rangle$.
- b) In polycrystalline materials, significant local stress concentrations is a common phenomenon during the deformation [8-10]. As illustrated in Fig. R3, our crystal plasticity finite element modeling of T1.2 highlighted regions near the grain boundaries experiencing Von Mises stress magnitudes amplifying up to 4.5 times the macroscopic stress. This local stress concentration could activate slip systems with high nucleation/gliding resistance.
- c) In certain crystallographic orientations, the Schmid factor for $\text{Pyr2}\langle c+a \rangle$ can potentially surpass that of $\text{Pyr1}\langle c+a \rangle$, leading to a higher resolved shear stress on the Pyr2 plane.
- d) Peierl stress is only a part of the dislocation gliding resistance. The dislocation gliding resistance evolves with the dislocation density and latent hardening. It could reduce the gap between $\text{Pyr1}\langle c+a \rangle$ and $\text{Pyr2}\langle c+a \rangle$.
- e) In the context of HCP materials, exemplified by Mg, non-basal slip typically presents a substantially higher slip resistance compared to basal slip. Nevertheless, abundant evidence attests to the occurrence of cross-slip between basal and non-basal planes [11-12].

Consequently, given that $\langle c+a \rangle$ dislocations are active on Pyr2 (Fig. 2(f)) and that these dislocations encounter lower resistance on Pyr1 (Fig. 4(e)), we anticipate the

potential for these dislocations on Pyr2 to cross-slip onto Pyr1 (similar to what we see in [1-4]). Some of the above discussion, together with the corresponding references, have been added to the revised manuscript.

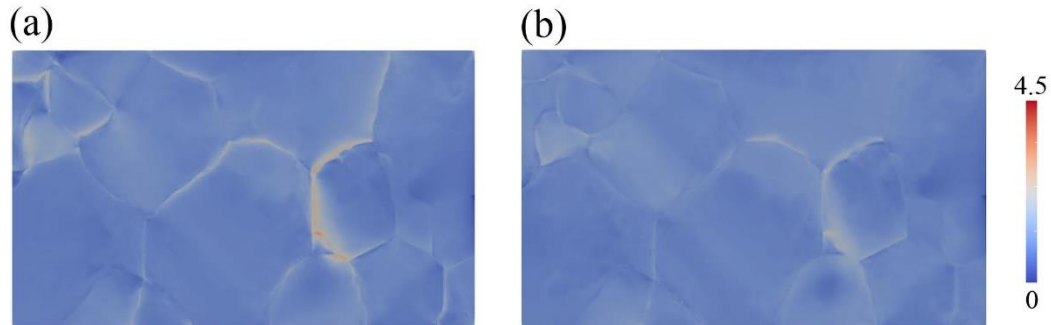


Fig. R3 Stress concentration map by CPFEM at $\epsilon = 0.064$: (a) pure Ti; (b) T1.2.

The color in the map represents the stress concentration (local Von Mises stress normalized by the macroscopic stress). The same microstructure was used for the two different specimen to rule out the impact of microstructure and texture. The critical stress and hardening parameters for T1.2 and pure Ti were obtained by fitting the experimental stress-strain curves. The enhanced $\langle c+a \rangle$ activity in T1.2 reduces the stress concentration near the grain boundaries.

Reference:

- [1] Sandlöbes, S., Friák, M., Zaeferrer, S., Dick, A., Yi, S.B., Letzig, D., Pei, Z.R., Zhu, L.F., Neugebauer, J. and Raabe, D., 2012. The relation between ductility and stacking fault energies in Mg and Mg–Y alloys. *Acta Materialia*, 60(6-7), pp.3011-3021.
- [2] Tang, Y. and El-Awady, J.A., 2014. Formation and slip of pyramidal dislocations in hexagonal close-packed magnesium single crystals. *Acta Materialia*, 71, pp.319-332.
- [3] Wu, Z. and Curtin, W.A., 2016. Mechanism and energetics of $\langle c+a \rangle$ dislocation cross-slip in hcp metals. *Proceedings of the National Academy of Sciences*, 113(40), pp.11137-11142.
- [4] Wu, Z., Ahmad, R., Yin, B., Sandlöbes, S. and Curtin, W.A., 2018. Mechanistic origin and prediction of enhanced ductility in magnesium alloys. *Science*, 359(6374), pp.447-452.
- [5] Fan, H. and El-Awady, J.A., 2015. Towards resolving the anonymity of pyramidal slip in magnesium. *Materials Science and Engineering: A*, 644, pp.318-324.
- [6] Agnew, S.R., Capolungo, L. and Calhoun, C.A., 2015. Connections between the basal II “growth” fault and $\langle c+a \rangle$ dislocations. *Acta Materialia*, 82, pp.255-265.
- [7] Basu, I., Chen, M., Wheeler, J., Schäublin, R.E. and Löffler, J.F., 2022. Segregation-driven exceptional twin-boundary strengthening in lean Mg–Zn–Ca alloys. *Acta Materialia*, 229, p.117746.
- [8] Koike, J., Kobayashi, T., Mukai, T., Watanabe, H., Suzuki, M., Maruyama, K. and Higashi, K., 2003. The activity of non-basal slip systems and dynamic recovery at room temperature in fine-grained AZ31B magnesium alloys. *Acta materialia*, 51(7), pp.2055-2065.
- [9] Abdolvand, H. and Wilkinson, A.J., 2016. On the effects of reorientation and shear transfer during twin formation: comparison between high resolution electron backscatter diffraction experiments and a crystal plasticity finite element model. *International Journal of Plasticity*, 84,

pp.160-182.

[10] Andani, M.T., Lakshmanan, A., Sundararaghavan, V., Allison, J. and Misra, A., 2020. Quantitative study of the effect of grain boundary parameters on the slip system level Hall-Petch slope for basal slip system in Mg-4Al. *Acta Materialia*, 200, pp.148-161.

[11] Zhu, G., Wang, L., Zhou, H., Wang, J., Shen, Y., Tu, P., Zhu, H., Liu, W., Jin, P. and Zeng, X., 2019. Improving ductility of a Mg alloy via non-basal slip induced by Ca addition. *International Journal of Plasticity*, 120, pp.164-179.

[12] Yasi, J.A., Hector Jr, L.G. and Trinkle, D.R., 2012. Prediction of thermal cross-slip stress in magnesium alloys from a geometric interaction model. *Acta materialia*, 60(5), pp.2350-2358.

6. This work aims to activate multi-slips to improve strength-toughness combination. However, the activation of multi-slips is expected to improve the plasticity, and sometimes increase the ductility which is reflected by the tensile elongation. Actually, toughness of the materials is not only influenced by the slip activities, but the work hardening behavior, effected by the interaction between the slips, or the GB behaviors, or the cracks behavior. And the plasticity and ductility were also mentioned several times throughout the manuscript. I think that some basic concepts are misunderstood, like plasticity, toughness or ductility. The main points of the paper should be corrected. Meanwhile, the paper aims to study multi-principle element alloys (MPEAs)—high alloy concentration and local fluctuation—on the toughness. However, the effect of the alloy concentration on the plastic deformation was not fully explained, since the difference between Ti1.0 and Ti1.2 alloy was not explored.

Response:

1) The reason why we focus on toughness instead of ductility:

One potential application of the Ti-Zr-Hf alloys is for medical use, given the recognized biocompatibility of its constituent elements. For such applications, a crucial requirement is energy absorption. This is the reason why in this work we focus on the (static) toughness of the material instead of its ductility, although the two properties are interconnected.

2) The concept of plasticity, ductility, and toughness:

The reviewer raised a very important point, which is to distinguish the three basic concepts of plasticity, ductility, and toughness. Following Zhu et al. [1], plasticity is

the ability of a solid material to undergo plastic deformation without fracture. Ductility is a material's ability to deform under tensile stress, and can be considered as a special case of plasticity: plasticity under tensile loading. Toughness is the ability of a material to absorb energy and plastically deform without fracturing. Following the reviewer's kind suggestion, the authors carefully checked the terminology used throughout the revised manuscript.

In this work the toughness refers to static toughness which is the area under the tensile stress-strain curves. The toughness is affected by the strength and ductility (elongation). Hence, in some places of the manuscript, we unavoidably mention the ductility and elongation. In the manuscript, the word "plasticity" is always preceded by the word "dislocation", and the phrase "dislocation plasticity" refers to a microscopic deformation mechanism instead of a material's macroscopic property (like plasticity, ductility, and toughness). Hopefully, these terms will not lead to any confusion for future readers.

3) Factors that affect the ductility and toughness:

We thank the reviewer for reminding us that the material's toughness is related to the work hardening. Fig. R4 is the work hardening curves of the three materials investigated in this work. It can be seen that the work hardening rate is markedly higher for the two HCP MPEAs than pure Ti. This justifies the superior toughness of the two MPEAs.

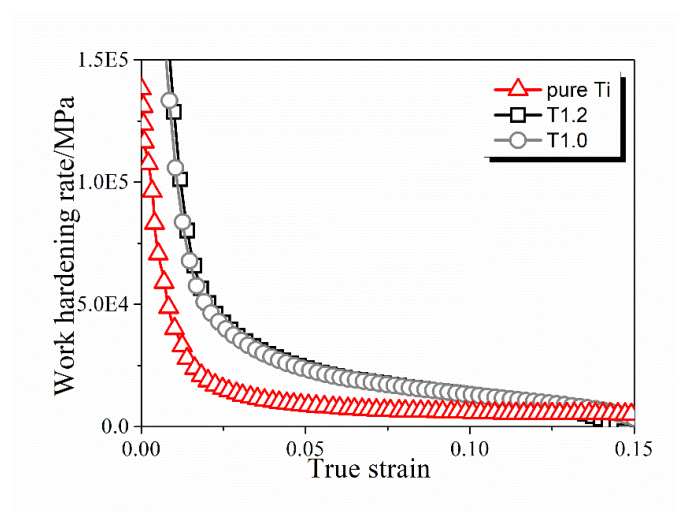


Fig. R4 Work hardening rate of T1.2, T1.0, and pure Ti

Concerning the intrinsic reason responsible for the above observed enhanced work hardening and, consequently, improved toughness, as mentioned by the reviewer, it could be related to factors including twinning, dislocation interaction, and grain boundary properties (crack behavior). Since the twin fraction is obviously lower in the two MPEAs than in pure Ti, we can easily conclude that the enhanced toughness in MPEA is not caused by twinning. In this regard, we focus on the dislocation activity and grain boundaries.

Regarding the dislocation activity, the wide distribution of F_{max} and τ_{pn} permits $\langle c+a \rangle$ dislocations to activate over a broad stress/strain window, ensuring that for every stress/strain increment within this range, there is always a portion of $\langle c+a \rangle$ dislocations ready to become active. This leads to continuous work hardening, akin to the multistage deformation observed in other high-entropy alloys [2, 3, 4], and results in a high work hardening rate. Additionally, the amplified Pyr1 and Pyr2 slip activity, in contrast to the deformation dominated by Prism $\langle a \rangle$, introduces significant latent hardening and enhances interactions among various slip modes/defects (validated by the increased dislocation density in MPEAs ($7\sim 11 \times 10^{14} \text{ m}^{-2}$) versus pure Ti ($\sim 4 \times 10^{14} \text{ m}^{-2}$)). This is also beneficial to elevating the work hardening rate [5, 6]. Furthermore, as the solute clusters could strengthen the dislocation junctions [7], they could potentially heightening dislocation interactions and boosting the work hardening even further. Moreover, the enhanced $\langle c+a \rangle$ activity helps to alleviate stress concentrations near grain boundaries [8, 9] (also evidenced by our CPFEM results, Fig. R3) and decrease the likelihood of grain boundary decohesion. Apparently, the synergy between the improved work hardening and more even stress distribution, both originated from the significantly more prevalent Pyr1 and Pyr2 slips in MPEA, contributes to the superior toughness observed in MPEAs relative to pure Ti.

With respect to the grain boundary, its impact can be analyzed by comparing the fracture surface of different alloys. As shown in Fig. R5, the annealed pure Ti presents typical ductile fracture, but when we cold-rolled the material to have a comparable strength with the MPEAs, it presented a brittle fracture, with many smooth

propagation paths and even complete original grain outlines. Such morphology indicates that the cracks are more likely to propagate along the grain boundaries rather than grain interiors at high stress. However, while having an even higher strength than that of cold-rolled Ti, the T1.2 presents a ductile fracture with many dimples and very few grain boundary cracks. The restrained grain boundary cracking (compared to cold-rolled Ti) here, on the one hand, should be related to the above-mentioned improved Pyr1 and Pyr2 slip activity which reduce the stress concentration near the grain boundaries, and on the other hand, should be related to a higher grain boundary strength in T1.2. Meanwhile, since some grain boundary cracks are indeed observed in T1.2, it is reasonable to state that the grain boundaries are actually weak points in this material. Hence, the enhanced grain boundary strength should have its positive influence, but it is unlikely to serve as the major contributor to the enhanced toughness observed in the two MPEAs. The authors believe that this is consistent with our literature survey in conventional HCP materials. Despite numerous works on FCC and BCC alloys focusing on the grain boundary [10-14], in HCP materials, when it comes to ductility and toughness, more emphasis is placed on the effect of $\langle c+a \rangle$ slip than on the grain boundaries (although they do not deny the latter also play a role) [15-19], with only a few exceptions [9, 20].

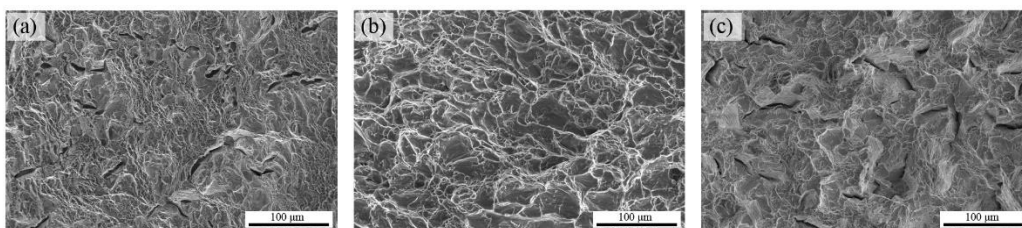


Fig. R5 Fracture surface:

(a) annealed T1.2; (b) annealed pure Ti; (c) cold-rolled pure Ti

Also it is worth mentioning here that, **inspired by the reviewer's comment, we have systematically compared the grain boundary parameters in MPEAs and pure Ti.** The results (provided in **Supplementary Materials**) turn out that the grain boundaries in the three specimens have no obvious differences in density (inferred from the similar grain size, **Fig. 1**), misorientation (inferred from misorientation distribution function,

Fig. S1), or tilt/twist character (inferred from angle between the misorientation axis and the 2D grain boundary segment, Fig. S2). Moreover, composition analysis yields no evidence of grain boundary segregation/precipitation in either of the MPEAs. This means that the higher grain boundary strength in T1.2 should arise from the intrinsic enhancement of the grain boundary cohesion, rather than the existence of any types of special grain boundaries. Moreover, we do not rule out the possibility that the alloy elements in MPEAs may reduce the vacancy diffusivity and hence delay the void nucleation/growth.

In summary, the improved toughness in MPEAs should arise primarily from the enhanced Pyr1 and Pyr2 slips which leads to higher work hardening and lower stress concentration near the grain boundaries. In addition, the increased grain boundary cohesion and the reduced vacancy diffusivity should also have some positive (but secondary) impact. **In pursuit of academic rigor and to present a holistic view, we have incorporated a succinct discussion encompassing these aspects in the revised manuscript to provide readers with a comprehensive understanding and to preempt potential ambiguities. We have also added some of the above results to the Supplementary Materials for readers who are interested in them.**

We would like to express our gratitude to the reviewer for his/her valuable insights, which helps us improve the quality of this manuscript.

4) Comparison between T1.0 and T1.2:

As mentioned in the previous response, since the dislocation behavior and mechanical properties of the two MPEAs are qualitatively similar, it is not our intention to find out the underlying reasons responsible for the difference between them. In fact, we studied the two intrinsic effects of MPEA, i.e..high alloy concentration and local fluctuation, via the comparison between T1.2 and pure Ti. More specifically, the leftmost subfigure in Fig. 4(d) and (e) (comparison between pure Ti and T1.2 in random solution state) demonstrate the effect of high alloy concentration on the restoring stress and the Peierls stress. Other subfigures in Fig. 4(d) and (e) (comparing solute fluctuation in different degrees) demonstrate the effect of solute fluctuation (different

σ). Incorporating the T1.0 data into this manuscript is only meant to let the readers know that the effect of high alloy concentration and solute fluctuation on the dislocation activities is not exclusive to the T1.2, but span the broader Ti-Zr-Hf system.

Considering that the DFT calculation taking solute fluctuation into account is computationally expensive, detailed investigation on the differences between various Ti-Zr-Hf alloys is far beyond the scope of the present short communication. It will be reported in the future in a full-length article. Some sentences have been added to emphasize to the readers that T1.0 and T1.2 are qualitatively similar in comparison to pure Ti, and that because of this, we use T1.2 as an example to shed light on the differences between the HCP MPEA and pure Ti.

Reference:

- [1a] Zhu, Y.T. and Wu, X.L., 2018. Ductility and plasticity of nanostructured metals: differences and issues. *Materials Today Nano*, 2, pp.15-20.
- [2] Li, Z., Pradeep, K.G., Deng, Y., Raabe, D. and Tasan, C.C., 2016. Metastable high-entropy dual-phase alloys overcome the strength–ductility trade-off. *Nature*, 534(7606), pp.227-230.
- [3] Naeem, M., He, H., Zhang, F., Huang, H., Harjo, S., Kawasaki, T., Wang, B., Lan, S., Wu, Z., Wang, F. and Wu, Y., 2020. Cooperative deformation in high-entropy alloys at ultralow temperatures. *Science Advances*, 6(13), p.eaax4002.
- [4] Zhang, D.D., Zhang, J.Y., Kuang, J., Liu, G. and Sun, J., 2021. Superior strength-ductility synergy and strain hardenability of Al/Ta co-doped NiCoCr twinned medium entropy alloy for cryogenic applications. *Acta Materialia*, 220, p.117288.
- [5] Syed, B., Geng, J., Mishra, R.K. and Kumar, K.S., 2012. [0 0 0 1] Compression response at room temperature of single-crystal magnesium. *Scripta Materialia*, 67(7-8), pp.700-703.
- [6] Basu, I., Chen, M., Wheeler, J., Sch äublin, R.E. and L öffler, J.F., 2022. Segregation-driven exceptional twin-boundary strengthening in lean Mg–Zn–Ca alloys. *Acta Materialia*, 229, p.117746.
- [7] Picu, R.C., 2004. A mechanism for the negative strain-rate sensitivity of dilute solid solutions. *Acta Materialia*, 52(12), pp.3447-3458.
- [8] Koike, J., Kobayashi, T., Mukai, T., Watanabe, H., Suzuki, M., Maruyama, K. and Higashi, K., 2003. The activity of non-basal slip systems and dynamic recovery at room temperature in fine-grained AZ31B magnesium alloys. *Acta materialia*, 51(7), pp.2055-2065.
- [9] Chong, Y., Gholizadeh, R., Tsuru, T., Zhang, R., Inoue, K., Gao, W., Godfrey, A., Mitsuhashi, M., Morris Jr, J.W., Minor, A.M. and Tsuji, N., 2023. Grain refinement in titanium prevents low temperature oxygen embrittlement. *Nature communications*, 14(1), p.404.
- [10] Zhang, S., Kontsevoi, O.Y., Freeman, A.J. and Olson, G.B., 2010. Sodium-induced embrittlement of an aluminum grain boundary. *Physical Review B*, 82(22), p.224107.
- [11] Geng, W.T., Freeman, A.J., Wu, R., Geller, C.B. and Reynolds, J.E., 1999. Embrittling and strengthening effects of hydrogen, boron, and phosphorus on a Σ 5 nickel grain boundary. *Physical Review B*, 60(10), p.7149.

- [12] Schweinfest, R., Paxton, A.T. and Finnis, M.W., 2004. Bismuth embrittlement of copper is an atomic size effect. *Nature*, 432(7020), pp.1008-1011.
- [13] Wu, R., Freeman, A.J. and Olson, G.B., 1994. First principles determination of the effects of phosphorus and boron on iron grain boundary cohesion. *Science*, 265(5170), pp.376-380.
- [14] Raabe, D., Herbig, M., Sandlöbes, S., Li, Y., Tytko, D., Kuzmina, M., Ponge, D. and Choi, P.P., 2014. Grain boundary segregation engineering in metallic alloys: A pathway to the design of interfaces. *Current Opinion in Solid State and Materials Science*, 18(4), pp.253-261.
- [15] Wu, Z. and Curtin, W.A., 2015. The origins of high hardening and low ductility in magnesium. *Nature*, 526(7571), pp.62-67.
- [16] Wang, H., Pan, R., Tang, A., She, J., Mi, X., Wu, L. and Tan, J., 2021. Effects of Nb concentration and temperature on generalized stacking fault energy of Zr–Nb alloys by molecular dynamics simulations. *Materials Research Express*, 8(1), p.016540.
- [17] Yu, Q., Sun, J., Morris Jr, J.W. and Minor, A.M., 2013. Source mechanism of non-basal $\langle c+a \rangle$ slip in Ti alloy. *Scripta Materialia*, 69(1), pp.57-60.
- [18] Sandlöbes, S., Pei, Z., Friák, M., Zhu, L.F., Wang, F., Zaeferrer, S., Raabe, D. and Neugebauer, J., 2014. Ductility improvement of Mg alloys by solid solution: Ab initio modeling, synthesis and mechanical properties. *Acta Materialia*, 70, pp.92-104.
- [19] Liu, S.Y., Zhang, J.Y., Kuang, J., Bao, X.Y., Zhang, D.D., Zhang, C.L., Yang, J.K., Liu, G. and Sun, J., 2022. Designing hetero-structured ultra-strong and ductile Zr-2.5 Nb alloys: Utilizing the grain size-dependent martensite transformation during quenching. *Journal of Materials Science & Technology*, 125, pp.198-211.
- [20] Zeng, Z.R., Bian, M.Z., Xu, S.W., Davies, C.H.J., Birbilis, N. and Nie, J.F., 2016. Effects of dilute additions of Zn and Ca on ductility of magnesium alloy sheet. *Materials Science and Engineering: A*, 674, pp.459-471.

Reviewer #2:

The present submission proposed a strategy that the two intrinsic properties of multi-principle element alloys (MPEAs)—high alloy concentration and local fluctuation—can work synergistically to narrow the gap in nucleation/glide resistance between non-prismatic slip and prismatic slip, leading to enhanced activities of and first order pyramidal dislocations. This leads to an exceptional strength-toughness combination. The topic is interesting and the result is new. I think it can be published after some minor revisions:

Response: We appreciate the reviewer's encouraging feedback.

1. To achieve a similar combination of strength and ductility, there has been many other methods, what is the advantage of your method. it is better the author point out this in the paper.

Response: We appreciate the reviewer's insightful suggestion. It's acknowledged that there exists a variety of methods to attain comparable mechanical properties in alloys. However, we'd like to underscore the distinct benefits inherent in our approach.

1) Enhanced capability of narrowing the gap among different slip modes in HCP alloys:

A prevailing challenge within the HCP materials community involves the modification of nucleation/glide resistance across different slip modes. This task is fundamental in optimizing the balance between strength, ductility, and toughness of the materials. While conventional alloying and precipitation strategies have shown some capability in addressing this concern, their potential to reduce the gap among different slip modes remains somewhat limited. In stark contrast, our approach, leveraging high alloy concentration coupled with solute fluctuations, exhibits a notable reduction in the Peierls stress ratio and thus a remarkable increase in $\langle c+a \rangle$ activity — a result which surpasses efficiencies reported by many traditional methodologies in literature.

2) Broad applicability:

The enhanced strength and toughness observed in T1.2 and T1.0 are

predominantly attributed to the increased activity of Pyr1 and Pyr2 slips. This modified slip behavior is a direct outcome of high solute concentration and solute fluctuation. As these two are fundamental characteristics of MPEAs, the methodology outlined in this work holds the potential for broad applicability across a diverse array of MPEAs. This stands in stark contrast to certain strategies that may only be effective for specific types of alloys.

3) **Compatible with other strategies:**

As demonstrated in our manuscript, the MPEAs evaluated in our study boast a simplified microstructure — fully recrystallized single-phase microstructure with coarse equiaxed grains. Although this microstructure may seem mechanically inferior when contrasted with intricate microstructures like gradient, laminate, bimodal, or multiscale structures, both T1.2 and T1.0 exhibit a remarkable balance of strength and toughness. These results rival many alloys that boast complex microstructures. This underscores that our approach sets a robust baseline. Building upon this foundation, further microstructural designs can potentially push these materials to achieve even superior mechanical properties. Essentially, the strategy we introduce in this study can be seamlessly integrated with other methodologies, paving the way for collaborative efforts to realize unparalleled material attributes.

Following the reviewer's kind suggestion, we have enriched the revised manuscript by expressly articulating the advantages of our method.

2. The ductility is related to many factors, including the activity of non-basal slip, fracture behavior, twinning deformation. The author should mention those and make a relevant discussion.

Response: We are grateful for the reviewer's insightful suggestion and fully concur with his/her assertion that the ductility of an HCP material is linked to slip activity, twinning behavior, and fracture behavior. In light of this, we have incorporated a succinct discussion into the revised manuscript to elucidate this.

Since the twin fraction is obviously lower in the two MPEAs than in pure Ti, we can easily deduce that it doesn't play a pivotal role in maintaining the ductility of

MPEAs at elevated stress levels. In this regard, our attention is drawn to dislocation activity and fracture behavior.

Regarding the dislocation activity, the wide distribution of F_{max} and τ_{pn} permits $\langle c+a \rangle$ dislocations to activate over a broad stress/strain window, ensuring that for every stress/strain increment within this range, there is always a portion of $\langle c+a \rangle$ dislocations ready to become active. This leads to continuous work hardening, akin to the multistage deformation observed in other high-entropy alloys [1, 2, 3], and results in a high work hardening rate. Additionally, the amplified Pyr1 and Pyr2 slip activity, in contrast to the deformation dominated by Prism $\langle a \rangle$, introduces significant latent hardening and enhances interactions among various slip modes/defects (validated by the increased dislocation density in MPEAs ($7\sim 11 \times 10^{14} \text{ m}^{-2}$) versus pure Ti ($\sim 4 \times 10^{14} \text{ m}^{-2}$)). This is also beneficial to elevating the work hardening rate [4, 5]. Furthermore, as the solute clusters could strengthen the dislocation junctions [6], they could potentially heightening dislocation interactions and boosting the work hardening even further. Moreover, the enhanced $\langle c+a \rangle$ activity helps to alleviate stress concentrations near grain boundaries [7, 8] (also evidenced by our CPFEM results, Fig. R6) and decrease the likelihood of grain boundary decohesion. Apparently, the synergy between the improved work hardening and more even stress distribution, both originated from the significantly more prevalent Pyr1 and Pyr2 slips in MPEA, contributes to the excellent strength-ductility combination and thus the superior toughness observed in MPEAs relative to pure Ti.

With respect to the fracture behavior, As shown in Fig. R7 (also given in Fig. S4), both pure Ti and T1.2 show ductile fracture characterized by the presence of dimples, albeit of varying depths. This highlights a consistent crack pattern across the two materials. In addition to dimples, the T1.2 also displays some grain boundary fractures with smooth progression paths. This is understandable considering the strength-ductility tradeoff, since the strength of T1.2 is markedly higher than that of pure Ti. To obtain further insight into the fracture of T1.2, we compared its fracture surface to that of a cold-rolled pure Ti with comparable strength. As shown in Fig.

R7(c), the cold-rolled Ti manifests a brittle fracture pattern, with many smooth propagation paths and even complete original grain outlines. This is in stark contrast with T1.2, suggesting that while having a high strength, the T1.2 are less susceptible to grain boundary cracking. This, on the one hand, should be related to the above mentioned improved Pyr1 and Pyr2 slip activity which reduce the stress concentration near the grain boundaries, and on the other hand, could be related to the improved grain boundary cohesion.

With the incorporation of key points mentioned above into the revised manuscript and Fig. R7 into the Supplementary Materials, we believe the paper has become more comprehensive and rigorous. We value the reviewer's insightful suggestions.

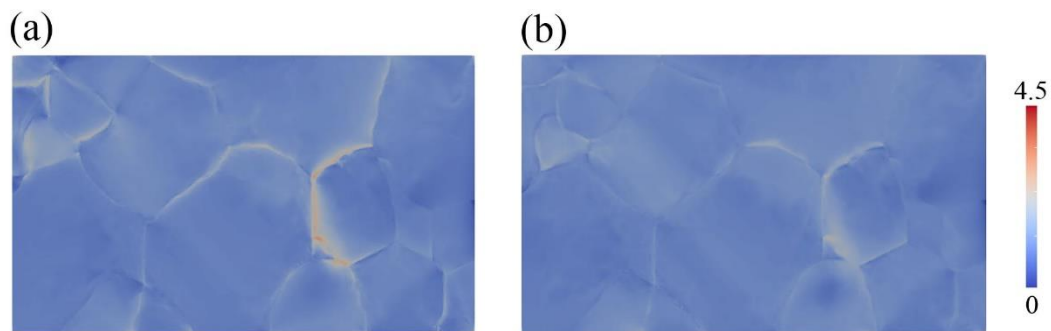


Fig. R6 Stress concentration map by CPFEM at $\epsilon = 0.064$: (a) pure Ti; (b) T1.2.

The color in the map represents the stress concentration (local Von Mises stress normalized by the macroscopic stress). The same microstructure was used for the two different specimen to rule out the impact of microstructure and texture. The critical stress and hardening parameters for T1.2 and pure Ti were obtained through fitting the experimental stress-strain curves. The enhanced $\langle c+a \rangle$ activity in T1.2 reduce the stress concentration near the grain boundaries.

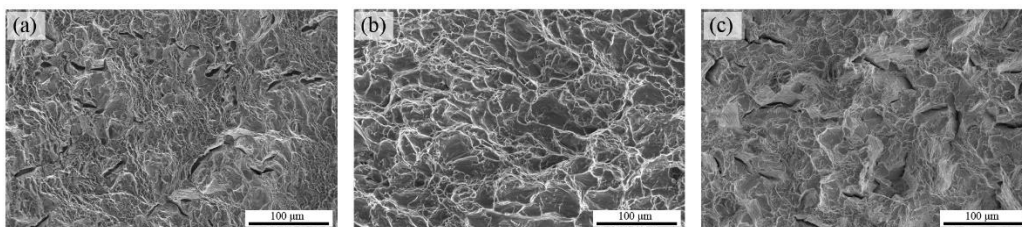


Fig. R7 Fracture surface:

(a) annealed T1.2; (b) annealed pure Ti; (c) cold-rolled pure Ti

Reference:

- [1] Li, Z., Pradeep, K.G., Deng, Y., Raabe, D. and Tasan, C.C., 2016. Metastable high-entropy dual-phase alloys overcome the strength–ductility trade-off. *Nature*, 534(7606), pp.227-230.
- [2] Naeem, M., He, H., Zhang, F., Huang, H., Harjo, S., Kawasaki, T., Wang, B., Lan, S., Wu, Z., Wang, F. and Wu, Y., 2020. Cooperative deformation in high-entropy alloys at ultralow temperatures. *Science Advances*, 6(13), p.eaax4002.
- [3] Zhang, D.D., Zhang, J.Y., Kuang, J., Liu, G. and Sun, J., 2021. Superior strength-ductility synergy and strain hardenability of Al/Ta co-doped NiCoCr twinned medium entropy alloy for cryogenic applications. *Acta Materialia*, 220, p.117288.
- [4] Syed, B., Geng, J., Mishra, R.K. and Kumar, K.S., 2012. [0 0 0 1] Compression response at room temperature of single-crystal magnesium. *Scripta Materialia*, 67(7-8), pp.700-703.
- [5] Basu, I., Chen, M., Wheeler, J., Sch äublin, R.E. and L öffler, J.F., 2022. Segregation-driven exceptional twin-boundary strengthening in lean Mg–Zn–Ca alloys. *Acta Materialia*, 229, p.117746.
- [6] Picu, R.C., 2004. A mechanism for the negative strain-rate sensitivity of dilute solid solutions. *Acta Materialia*, 52(12), pp.3447-3458.
- [7] Koike, J., Kobayashi, T., Mukai, T., Watanabe, H., Suzuki, M., Maruyama, K. and Higashi, K., 2003. The activity of non-basal slip systems and dynamic recovery at room temperature in fine-grained AZ31B magnesium alloys. *Acta materialia*, 51(7), pp.2055-2065.
- [8] Chong, Y., Gholizadeh, R., Tsuru, T., Zhang, R., Inoue, K., Gao, W., Godfrey, A., Mitsuhashi, M., Morris Jr, J.W., Minor, A.M. and Tsuji, N., 2023. Grain refinement in titanium prevents low temperature oxygen embrittlement. *Nature communications*, 14(1), p.404.

3. *What is the relation between the strength and activity of non-basal slips. It increase or reduce the strength.*

Response: We thank the reviewer for raising this question. We understand that by non-basal slip, the reviewer refers to the pyramidal $\langle c+a \rangle$ slips (because in pure Ti and Ti-Zr-Hf MPEAs, the prism $\langle a \rangle$ slip has the lowest nucleation/glide resistance and $\langle c+a \rangle$ slip has the largest). Regarding the strength of the material, we believe that it is multifaceted, depending both on the activity and the nucleation/gliding resistance of $\langle c+a \rangle$ slip systems. Therefore, it is difficult to say in a general sense that there is a positive or negative correlation between the $\langle c+a \rangle$ slip activities and the strength of the material. Our detailed understanding is provided below.

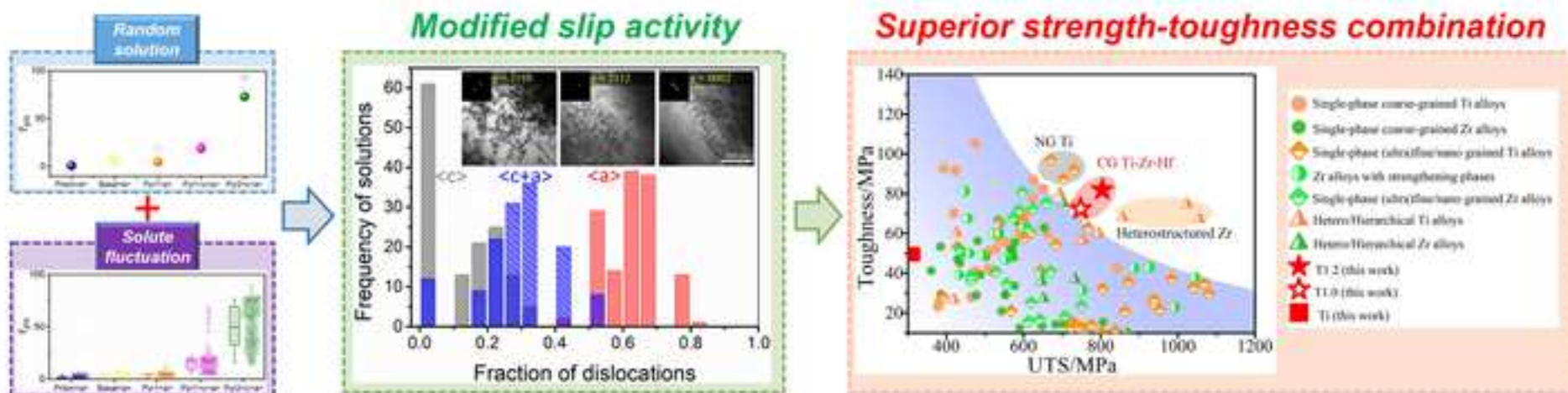
In HCP materials, $\langle c+a \rangle$ is the sole slip dislocation type, as opposed to twinning, that will enable c axis deformation of the crystal. So if, for instance, when twinning is impeded due to certain microstructural characteristics, either the initiation/propagation

of cracks or the engagement of $\langle c+a \rangle$ slips is necessitated. The choice between these processes hinges on their respective energy requirements.

In scenarios where crack nucleation and propagation are energetically favorable at lower stress levels, the material demonstrates low $\langle c+a \rangle$ activity and low strength. Conversely, when the activation of $\langle c+a \rangle$ slips is more energetically favorable, the material's strength is predominantly determined by the nucleation/gliding resistance of $\langle c+a \rangle$. A higher resistance correlates with increased material strength, and in this context, increased $\langle c+a \rangle$ activity is therefore associated with enhanced strength. However, if the nucleation/gliding resistance is low, the material might exhibit enhanced $\langle c+a \rangle$ activity but relatively low strength.

In our MPEAs, solute fluctuation leads to a distribution in the nucleation/gliding resistance of $\langle c+a \rangle$ slips, as illustrated in **Fig. 4(d) and (e)**. This distribution allows for the activation of $\langle c+a \rangle$ slips across a broad stress range, ensuring that for every stress increment within this range, a portion of $\langle c+a \rangle$ dislocations are ready to become active. This not only mitigates stress concentrations effectively, preventing crack initiation/propagation but also ensures a high work hardening and material strength. Hence, in the context of our study, increased $\langle c+a \rangle$ activity is associated with enhanced material strength.

Inspired by the reviewer's question, some of the above discussions are included in the revised manuscript to provide the readers with a clearer understanding on this topic.



Abstract

To effectively bolster $\langle c+a \rangle$ slip is pivotal to improving the mechanical property of hexagonal close-packed (HCP) metallic materials. It has been a longstanding challenge facing the structural material community. Here we introduce a strategy to crack this hard nut. Employing two coarse-grained Ti-Zr-Hf model alloys as examples, we demonstrate for the first time that the two intrinsic properties of multi-principle element alloys (MPEAs)—high alloy concentration and local fluctuation—can work synergistically to narrow the gap in nucleation/gliding resistance between non-prismatic slip and prismatic slip, leading to enhanced activities of $\langle c+a \rangle$ and first order pyramidal $\langle a \rangle$ dislocations. This renders the material an exceptional strength-toughness combination, outperforming other coarse-grained HCP alloys and even rivalling most of those with delicately designed microstructures including nanostructures and heterostructures. Given the high concentration and local fluctuation are intrinsic to all MPEAs, we anticipate that this strategy could extend to other MPEAs featuring an HCP structure.

Keywords hexagonal-close packed structure; multi-principle element alloys; dislocation plasticity; generalized stacking fault energy; strength-toughness combination

The mechanical properties of hexagonal close-packed (HCP) metals and alloys hinge on accommodating strains along the c-axis [1-3], usually through $\langle c+a \rangle$ slip or twinning—in most cases $\{10\bar{1}2\} \langle \bar{1}011 \rangle$ extension twins and $\{11\bar{2}2\} \langle 11\bar{2}\bar{3} \rangle$ contraction twins [4-6]. Taking pure Ti and its alloys as an example, twin-dominated mechanisms usually grant ductility at the expense of strength. Conversely, when twinning is suppressed, the c-axis strain must be borne by $\langle c+a \rangle$ slip [4, 7], which, with a high activation threshold stress, seldom becomes significantly active and are typically confined to areas of stress concentration [3, 8, 9]. Consequently, while $\langle c+a \rangle$ slip theoretically could accommodate c-axis strain, in practice, suppressing twinning and

1 relying on $\langle c+a \rangle$ slip for strain accommodation often, if not always, results in increased
2 strength but diminished ductility and toughness [6, 10-12]. The limited/insufficient
3 activation of $\langle c+a \rangle$ slip is the fundamental reason behind this age-old dilemma.
4 Addressing this traditional challenge in HCP materials calls for triggering widespread
5 and uniform $\langle c+a \rangle$ slip.
6
7
8
9

10 The most commonly employed method for boosting the $\langle c+a \rangle$ activity is through
11 (micro-)alloying [13-18]. The possible mechanisms behind the alloying effect include
12 reduced c/a ratio [19, 20], decreased I_1 stacking fault energy (SFE) [21, 22], delayed
13 basal transformation of $\langle c+a \rangle$ dislocations [23], promoted (double) cross-slip between
14 $\{10\bar{1}1\}$ (Pyr1) and $\{11\bar{2}2\}$ (Pyr2) [24], etc. However, in conventional alloys, the
15 solubility of alloying elements is often limited, and the presence of multiple elements
16 can lead to compound formation and solute segregation, reducing the solute
17 concentration in the matrix [25-27]. Consequently, attempts to enhance $\langle c+a \rangle$ activity
18 through solid solution often does not yield satisfactory results. Moreover, in some
19 extreme cases, while alloying can enhance $\langle c+a \rangle$ activity via narrowing the
20 activation/gliding resistance gap among different slip modes, it also lowers the
21 threshold stress of the harder deformation modes [28, 29]. Thus, it compromises the
22 desired strength-ductility balance while improving ductility.
23
24
25
26
27
28
29
30
31
32
33
34
35
36

37 In this study, we draw inspiration from the concept of multi-principal element
38 alloys (MPEAs) to propose a new strategy aimed at cracking the above hard nut. This
39 approach leverages two inherent MPEA characteristics—high alloy concentration and
40 local fluctuation—to enhance $\langle c+a \rangle$ slip in HCP alloys. Through systematic
41 investigation of coarse-grained Ti-Zr-Hf model alloys, we delve into the distinctive
42 dislocation plasticity in HCP MPEAs. Then we further elaborate on its role in achieving
43 an exceptional balance of strength and ductility, and consequently an outstanding
44 strength-toughness combination. This work is the first to report the influence of solute
45 fluctuation on the activation/gliding resistance gap among different slip modes in HCP
46 alloys. The findings are expected to shed new light on enhancing the mechanical
47 performance of not only single-phase HCP alloys, but also dual/multi-phase structures
48 containing HCP phases.
49
50
51
52
53
54
55
56
57
58
59
60
61
62
63
64
65

1 Two Ti-Zr-Hf model alloys ($\text{Ti}_{1.2}\text{Zr}_1\text{Hf}_1$ and $\text{Ti}_1\text{Zr}_1\text{Hf}_1$, in atomic ratio, denoted as
2 T1.2 and T1.0 hereafter) and pure Ti were casted by arc-melting. The c/a ratios of T1.2,
3 T1.0, and Ti are 1.586, 1.584, and 1.587, respectively, determined by X-ray diffraction
4 (XRD). For easy comparison, we controlled the thermomechanical processes to achieve
5 in the three materials comparable average grain sizes, nearly identical basal textures
6 and grain boundary characters (Fig. 1(a~b) and Fig. S1~S2). Readers are referred to
7 **Supplementary Materials** for more details of the experiments. Displayed in Fig. 1(d) is
8 the stress-strain curves of the three materials tested along the rolling direction (RD). It
9 reveals a marked increase in strength (~265%) and modest decrease in ductility (~40%)
10 in the MPEAs compared to pure Ti (Fig. 1(d)). When plotting the static toughness and
11 ultimate tensile strength (UTS) of various HCP materials in an Ashby map (Fig. 1(e)),
12 we found that the present MPEAs outperform not only all other existing coarse-grained
13 HCP counterparts (with or without strengthening phases) [5, 8, 30-53], but also,
14 surprisingly, the majority of those with ultrafine/nanograins [8, 32-34, 36, 37, 42, 43,
15 46, 47, 54-61] or hetero/hierarchical structures [5, 8, 31, 40, 43, 45, 62, 63]. In fact,
16 with coarse-grain structures, the two MPEAs even achieve similar properties to the
17 best-performing nanograined (NG) Ti and heterostructured Zr. This indicates the
18 potential for further property enhancement towards the upper-right corner of Fig. 1(e)
19 through microstructure engineering, a topic beyond the scope of this paper.
20
21
22
23
24
25
26
27
28
29
30
31
32
33
34
35
36
37
38
39
40
41
42
43
44
45
46
47
48
49
50
51
52
53
54
55
56
57
58
59
60
61
62
63
64
65

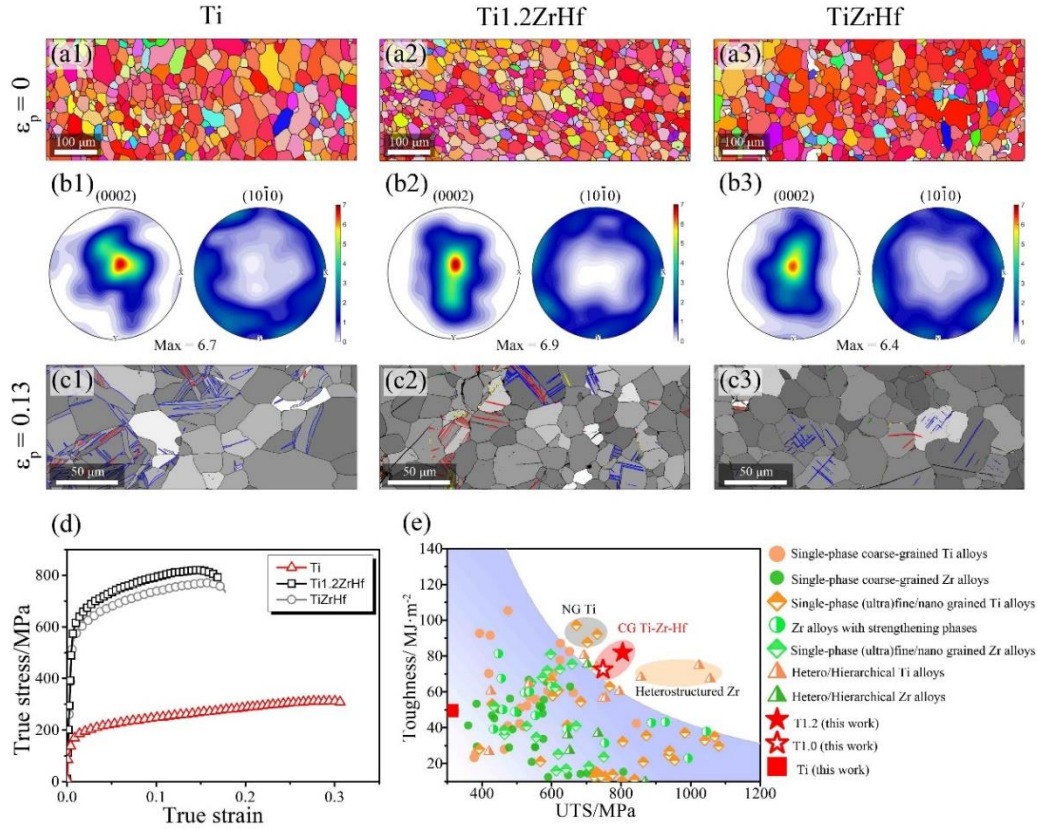


Fig. 1 Microstructure and mechanical properties of Ti, T1.2, and T1.0: (a) microstructure at $\varepsilon_p = 0$ (EBSD IPF map in ND); (b) texture at $\varepsilon_p = 0$ ($\{0002\}$ and $\{10\bar{1}0\}$ pole figures); (c) microstructure at $\varepsilon_p = 0.13$, the blue, red, and yellow lines correspond to $\{11\bar{2}2\} \langle 11\bar{2}\bar{3} \rangle$, $\{10\bar{1}2\} \langle \bar{1}011 \rangle$, and $\{11\bar{2}1\} \langle \bar{1}\bar{1}26 \rangle$ twins, respectively; (d) stress-strain curves along RD; (e) strength-toughness Ashby map. The subfigures with labels 1, 2, and 3 correspond to Ti, T1.2, and T1.0, respectively. In (e), different colors and shapes are used to represent the chemical composition and the microstructure, respectively. The data points are obtained from Ref. [5, 8, 30-63].

Given the similar microstructures, textures, and grain boundaries in the MPEAs and pure Ti, the observed enhancement in mechanical properties of the MPEAs should be something intrinsic. To unravel the underlying physics of this enhancement, we first examined the microstructure of the materials stretched to a true plastic strain of 0.13 ($\varepsilon_p = 0.13$), immediately before necking in the MPEAs. As shown in Fig. 1(c), pure Ti manifests a high fraction of thick-lenticular $\{11\bar{2}2\} \langle 11\bar{2}\bar{3} \rangle$ contraction twins, whereas the MPEAs exhibit a mix of both thin-elongated $\{11\bar{2}2\} \langle 11\bar{2}\bar{3} \rangle$

1 contraction twins and $\{10\bar{1}2\} \langle \bar{1}011 \rangle$ extension twins. Since slip and twinning, as
2 two major plastic carriers in metallic materials, collaboratively contribute to the
3 macroscopic strain [64], the contrast in twinning between Ti and MPEAs under the
4 same external conditions suggests differing dislocation plasticity in the two types
5 materials [65, 66]. This is the main focus of the present study.
6
7
8
9

10 **Fig.2** presents the key findings of the quasi-in-situ slip trace analysis. **Surface**
11 **morphology observations reveal that the slip traces in MPEAs are finer and more**
12 **abundant compared to those in pure Ti. Considering the $h = n \cdot |\vec{b}|$ relation (where h**
13 **denotes the height of the slip step, n the number of dislocations leaving the surface,**
14 **and \vec{b} the Burgers vector), this observation indicates a less concentrated and more**
15 **spread-out deformation (in mesoscale) in the MPEAs with lower individual shear strain**
16 **borne by each slip plane.** Notably, the chart in **Fig. 2(f)** illustrates the prevalent $\{10\bar{1}0\}$
17 prismatic (Prism) dislocation activities in both MPEAs and pure Ti, with the latter
18 showing higher Prism slip trace fractions. This is corroborated by the intragranular
19 misorientation axis (IGMA) analysis depicted in **Fig. 2(g)** where all three materials
20 exhibit concentrated peaks at/near $\langle 0001 \rangle$, with peak intensities decreasing from pure
21 Ti to T1.0 and T1.2. In contrast to the Prism slip traces, notably higher numbers of Pyr1
22 and Pyr2 slip traces are observed in the MPEAs than in pure Ti, indicating enhanced
23 pyramidal dislocation activities in the former.
24
25
26
27
28
29
30
31
32
33
34
35
36
37
38
39
40
41
42
43
44
45
46
47
48
49
50
51
52
53
54
55
56
57
58
59
60
61
62
63
64
65

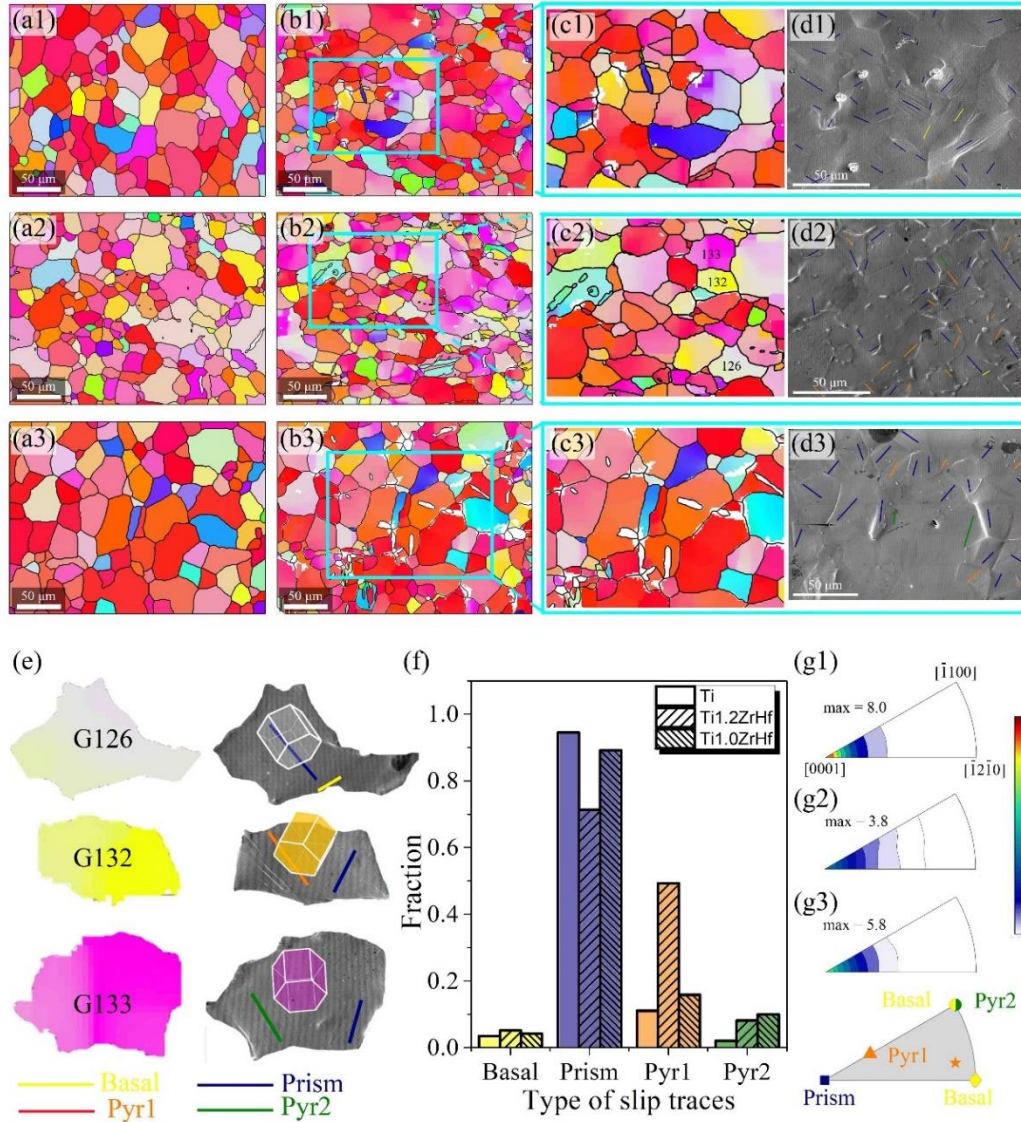


Fig. 2 Results of slip trace analysis: (a) EBSD ND-IPF map at $\epsilon_p=0$; (b) EBSD ND-IPF map at $\epsilon_p=0.08$; (c) magnified view of the area highlighted by the cyan rectangle in (b). (d) SEM surface morphology of the same area as (c). (e) slip trace identification for three representative grains in T1.2; (f) bar chart showing the number fraction of grains that exhibit the corresponding slip traces; (g) IGMA distribution. The subfigures with labels 1, 2, and 3 correspond to Ti, T1.2, and T1.0, respectively. The yellow, navy, orange, and olive lines in (d) and (e) represent the theoretical traces for Basal, Prism, Pyr1, and Pyr2 planes, respectively. Note that (a~d) are only one of the many regions tracked in this work. The statistical results provided in (f), however, are based on a total area of $\sim 800 \times 300 \text{ mm}^2$ and covers ~ 500 grains. The triangle placed below (g3) shows the theoretical positions of the IGMA for Prism<a>, Basal<a>, Pyr1<a>,

Pyr1<c+a>, and Pyr2<c+a>.

While the above SEM-based slip trace analysis provides reliable statistical data, it lacks Burgers vector information. To bridge this gap, convolutional multiple whole profile (CMWP) [67] and B2C analysis [68] were applied to reveal the dislocation density and Burgers vector distribution (Fig. 3). At $\varepsilon_p = 0.08$, MPEAs display dislocation densities of $7\sim 11 \times 10^{14} m^{-2}$, markedly surpassing that of pure Ti ($\sim 4 \times 10^{14} m^{-2}$). Moreover, the proportions of Burgers vectors (<a>, <c>, and <c+a>) varies across the materials. In pure Ti, <a> dislocations account for $\sim 72\%$ of total dislocations, while in T1.2 and T1.0, the value decreases to $\sim 61\%$ and $\sim 65\%$, respectively. Conversely, <c+a> dislocations constitute a mere $\sim 19\%$ in pure Ti, but goes up to $\sim 28\%$ for T1.2 and $\sim 25\%$ for T1.0.

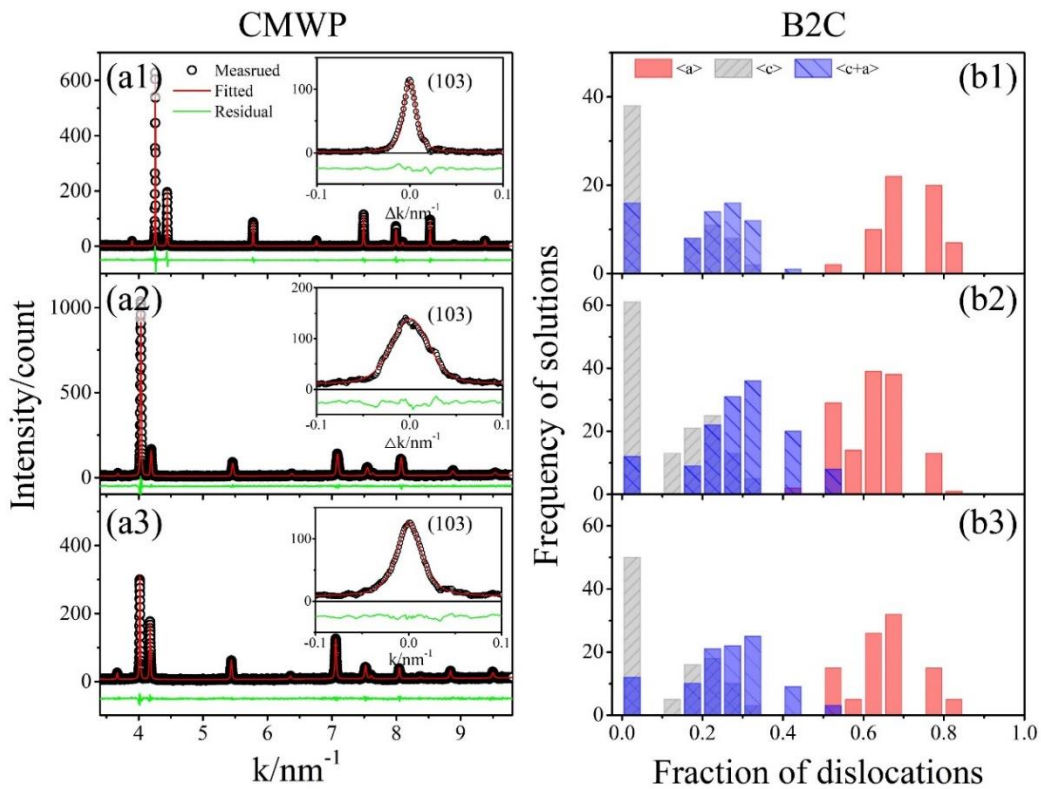


Fig. 3 Results of XRD-based dislocation analysis at $\varepsilon_p=0.08$: (a) measured and CMWP fitted diffraction profiles; (b) histograms of the frequency distributions of the valid solutions of <a>, <c>, and <c+a> dislocation fractions. The subfigures with labels 1, 2, and 3 correspond to Ti, T1.2, and T1.0, respectively. In (a), the light green curves represent the difference between the measured profile and the fitted one. In (b), the

1 centers of gravity of the histograms in red, gray, and blue are regarded as the relative
2 fractions of $\langle a \rangle$, $\langle c \rangle$, and $\langle c+a \rangle$ dislocations.
3

4
5 As Pyr2 slip traces can be only produced by slip system $\{11\bar{2}2\} \langle 11\bar{2}\bar{3} \rangle$ (Pyr2)
6 [69], the more profuse Pyr2 slip traces in T1.2 and T1.0 indicate higher Pyr2 $\langle c+a \rangle$
7 activities in the MPEAs compared to pure Ti. Given that the $\langle c+a \rangle$ dislocation fractions
8 are slightly higher, yet the Pyr2 slip trace fractions are marginally lower in T1.2 than in
9 T1.0, it is inferred that the Pyr1 $\langle c+a \rangle$ is more active in T1.2 than in T1.0. It is worth
10 mentioning that while this disparity should yield more Pyr1 slip traces in T1.2 than in
11 T1.0, it alone is insufficient to explain the threefold increase in the former. Hence, the
12 disparity in Pyr1 slip trace fractions must be attributed, at least partly, to Pyr1 $\langle a \rangle$.
13 Therefore, combining the slip trace and CMWP results, we conclude that compared
14 with pure Ti, the MPEAs not only demonstrate enhanced Pyr2 $\langle c+a \rangle$ and Pyr1 $\langle c+a \rangle$
15 activities but also more prevalent Pyr1 $\langle a \rangle$ slips, particularly evident in T1.2.
16
17

18
19
20
21
22
23
24
25
26
27
28 Generalized stacking fault energy (GSFE) curve is a useful tool for elucidating the
29 connection between composition-related features and the distinctive dislocation
30 plasticity [15, 70, 71]. Considering the similarities between T1.0 and T1.2, we selected
31 T1.2 as a representative Ti-Zr-Hf MPEA and examined its GSFE curves across five
32 typical slip modes, juxtaposed with those of pure Ti (Fig. 4(a)). Following Zhang et al.
33 [72] and assuming normal distributions of the GSFE in the present MPEAs, the
34 restoring stress (F_{max}) and the Peierls-Nabarro stress (τ_{pn}) of the MPEAs in different
35 fluctuation levels can be calculated. As shown in Fig. 4(b~c), with GSFE fluctuations,
36 F_{max} and τ_{pn} are no longer deterministic values (as is the case with conventional
37 alloys and ideally randomized MPEAs). Instead, for each slip mode, F_{max}
38 demonstrates a symmetric probability distribution whereas τ_{pn} a bias probability
39 distribution. In both cases, the distribution width expands with increasing GSFE
40 variance σ . Considering that F_{max} measures the difficulty in dislocation nucleation
41 and τ_{pn} the gliding resistance, the findings are consistent with the wavy morphology
42 and jerky motion of dislocations in MPEAs [73, 74].
43
44
45
46
47
48
49
50
51
52
53
54
55
56
57
58

59 Normalizing the F_{max} and τ_{pn} of various slip systems with those of Prism $\langle a \rangle$,

1 we obtain the relative restoring stress (\tilde{F}_{max}) and relative Peierls-Nabarro stress ($\tilde{\tau}_{pn}$)
2
3 (Fig.4(d~e)). The results show that in pure Ti, \tilde{F}_{max} and $\tilde{\tau}_{pn}$ are 1 : 1.7 : 2.7 : 2.7 :
4
5 2.8 and 1 : 11.1 : 18.8 : 21.5 : 93.7 , respectively, for
6
7 Prism<a>:Basal<a>:Pyr1<a>:Pyr1<c+a>:Pyr2<c+a>. As for T1.2 random solution,
8
9 however, the corresponding ratios become 1 : 1.1 : 2.1 : 2.5 : 2.7 and 1 : 6.0 : 4.7 :
10
11 19.0 : 73.0. Furthermore, starting from the random solution state ($\sigma = 0$), when GSFE
12
13 fluctuation is introduced to T1.2, it leads to not only scattering \tilde{F}_{max} and $\tilde{\tau}_{pn}$ values,
14
15 but also descending average $\tilde{\tau}_{pn}$ (Fig. 4(d~e)). At $\sigma = 0.10$, for instance, the ratio
16
17 decreases to 1 : 4.4 : 4.3 : 16.5 : 50.2. This suggests that, unlike conventional alloys
18
19 where the \tilde{F}_{max} and $\tilde{\tau}_{pn}$ are controlled only by the **global composition** [75], in
20
21 MPEAs, the impact of local fluctuations cannot be disregarded, and it scales with the
22
23 fluctuation level. For a detailed comparison on the relative contribution of global
24
25 composition and local fluctuation to the reduction of $\tilde{\tau}_{pn}$ at different fluctuation levels,
26
27 readers are directed to Fig. S3. We point out here that in the context of Ti-Zr-Hf MPEAs,
28
29 these two effects act in concert to promote the nucleation and glide of non-Prism slip
30
31 systems.
32
33
34
35
36
37
38
39
40
41
42
43
44
45
46
47
48
49
50
51
52
53
54
55
56
57
58
59
60
61
62
63
64
65

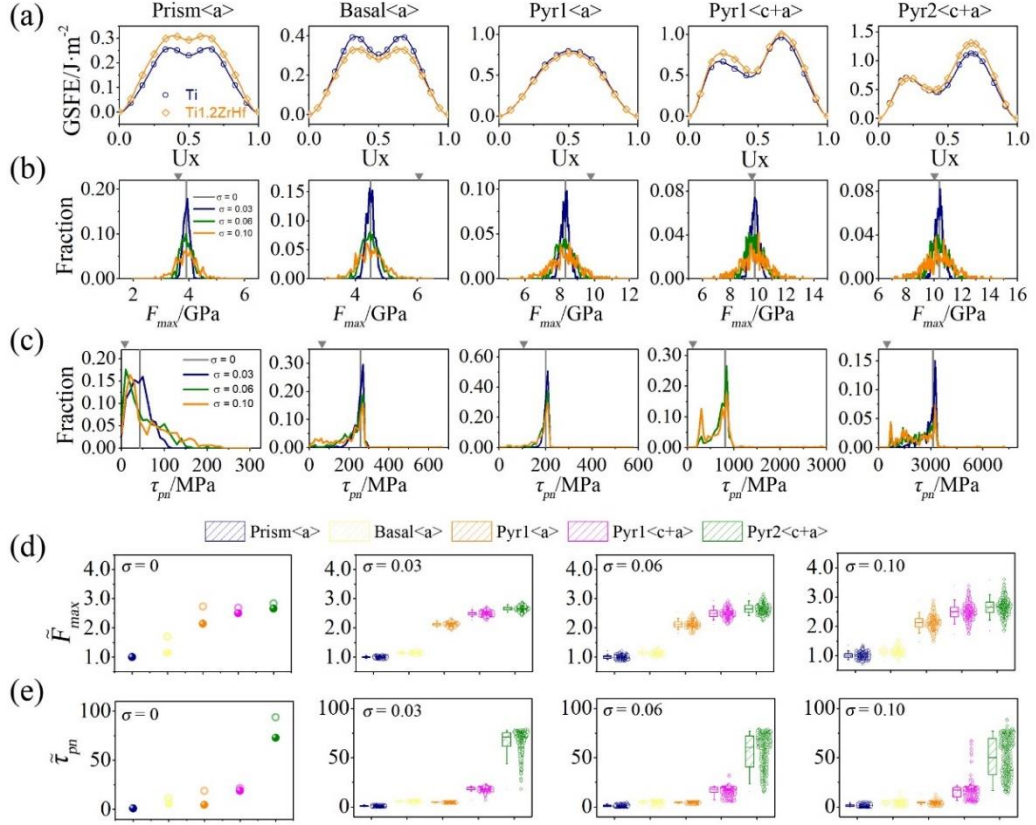


Fig. 4 Dislocation plasticity analysis based on GSFE curves: (a) GSFE curves; (b) distribution of F_{max} caused by local fluctuation; (c) distribution of τ_{pn} caused by local fluctuation; (d) variation of \tilde{F}_{max} with respect to local fluctuation. (e) variation of $\tilde{\tau}_{pn}$ with respect to local fluctuation. Gray arrowheads in (b) and (c) correspond to the values of pure Ti. In (d) and (e), for the subfigures $\sigma = 0$, the empty circle correspond to pure Ti, the solid circle correspond to T1.2 in random solution state.

More insights into the physical mechanisms behind the non-Prism slip activities in MPEAs can be achieved by cross-correlating the experimental and simulation results. As the \tilde{F}_{max} of Basal<a> is noticeably reduced, one might intuitively expect easier Basal<a> nucleation in MPEAs than in pure Ti. However, since the basal texture allows very small resolve shear stress on the basal plane, and that the $\tilde{\tau}_{pn}$ of Basal<a> is only marginally “softened” by Zr and Hf additions, Basal<a> dislocations, even if nucleated, were unlikely to glide in large scale. Thus, while this may appear counterintuitive, the small \tilde{F}_{max} and $\tilde{\tau}_{pn}$ of Basal<a> in T1.2 did not lead to high Basal<a> activity in this work.

1 It is noteworthy that while Basal<a> slip itself does not contribute noticeably to
2 the macroscopic strain, the propensity of basal stacking fault formation is closely tied
3 to <c+a> dislocation nucleation [21, 76, 77]. This association justifies the significantly
4 enhanced <c+a> activity in MPEAs compared to pure Ti, despite that the \tilde{F}_{max} of
5 Pyr1<c+a> and Pyr2<c+a> only decrease by ~7% and ~5%, respectively. Furthermore,
6 while Pyr1<c+a> is less sensitive to Zr and Hf addition compared to Pyr2<c+a>, its
7 $\tilde{\tau}_{pn}$ is far lower than that of Pyr2<c+a>. Hence, it is reasonable to speculate that a large
8 number of <c+a> dislocations, even if initially nucleated and glided on Pyr2, are likely
9 to cross-slip onto Pyr1 especially when encountering obstacles. The cross-slip
10 mechanism should be similar to those reported in the literature [1, 24, 78]. This Pyr2-
11 to-Pyr1 <c+a> cross-slip, along with the notably reduced \tilde{F}_{max} and $\tilde{\tau}_{pn}$ of Pyr1<a>,
12 explain the more prevalent Pyr1 slip in MPEAs compared to pure Ti. Besides, the strong
13 interaction between Pyr1<a> and <c+a> are expected to promote double cross-slip and
14 dislocation multiplication. This in turn contributes to a higher dislocation density and
15 better plastic homogeneity in the MPEAs, as evidenced by the CMWP and slip trace
16 results, respectively.

17 Dislocation activities play a critical role in determining the mechanical properties.
18 As shown in Fig. 4(b~c), for the primary slip system Prism<a>, the MPEAs have
19 notably higher F_{max} and τ_{pn} values compared to pure Ti, owing to solution
20 hardening. Together with the increased dislocation density, this explains the greater
21 strength of the MPEAs. The intriguing part here, however, is how the Ti-Zr-Hf MPEAs
22 manage only a slight dip in ductility while significantly enhancing strength, leading to
23 a superior strength-toughness combination. Clues lie in Fig. 5, showing that, unlike
24 pure Ti which at $\varepsilon_p = 0.02$ presents only <a> dislocations, the MPEAs display defects
25 aligned with basal traces, with Burgers vectors exhibiting both <a> and <c>
26 components. These are usually interpreted as either dissociated <c+a> dislocations [23,
27 79] or I_1 stacking faults serving as precursors to them [21, 76, 77]. Although it is
28 currently unclear which of these two explanations applies here, these basal defects are
29 considered immobile [24]. Given that all samples have a basal texture, they need either

1 {11 $\bar{2}2$ } < 11 $\bar{2}3$ > contraction twins or <c+a> dislocations to accommodate the
2 compressive strain in the thickness direction (ND). In pure Ti, {11 $\bar{2}2$ } < 11 $\bar{2}3$ >
3 contraction twins are activated at low stress levels, preventing the activation of <c+a>
4 dislocations on a large scale and resulting in low strength. The easy twin propagation
5 in pure Ti contributes to ductility but not toughness. In contrast, the MPEAs with their
6 rugged energy landscape hindering twin propagation [73, 80], make <c+a> dislocations,
7 which require higher stress to activate, the primary mechanism for accommodating the
8 compressive strain in ND. Upon loading, the MPEAs exhibit a progressive rise in flow
9 stress that either transforms the basal defects into mobile <c+a> dislocations [23] or
10 generates new ones [21, 76, 77]. With the wide distribution of F_{max} and τ_{pn} , <c+a>
11 dislocations are activated over a broad stress/strain window, ensuring that for every
12 stress/strain increment within this range, there is always a portion of <c+a> dislocations
13 ready to become active, leading to continuous work hardening. This mechanism,
14 resembling multistage deformation seen in other high-entropy alloys [81-83],
15 effectively mitigate stress concentrations. Besides, together with the pronounced latent
16 hardening (stemming from the activation of multiple slip modes) and the high-strength
17 dislocation junctions (attributable to high solute concentration and clustering [84]), it
18 significantly improves the work hardening rate of the MPEAs.

19 The homogeneous stress distribution and high work hardening rate, induced both
20 by the modified dislocation plasticity, are considered as the primary reason responsible
21 for the best-ever strength-toughness combination reported in coarse-grained HCP
22 materials. Yet, it's important to recognize that beyond the nucleation/gliding resistance
23 gap among the soft and hard slip modes, which typically dominates in HCP materials,
24 other factors can significantly influence the mechanical behavior as well [18, 85]. For
25 instance, comparing the ductile fracture of T1.2 to the brittle fracture of similarly strong,
26 cold-rolled pure Ti (Supplementary Materials) reveals the former's better grain
27 boundary cohesion, which also contributes to strength-toughness. Moreover, the
28 inherent lower vacancy diffusivity in MPEAs, which potentially hinders void formation
29 and growth, is another likely factor in toughness enhancement. Apparently, a more in-
30 depth exploration of these aspects is warranted in future research.

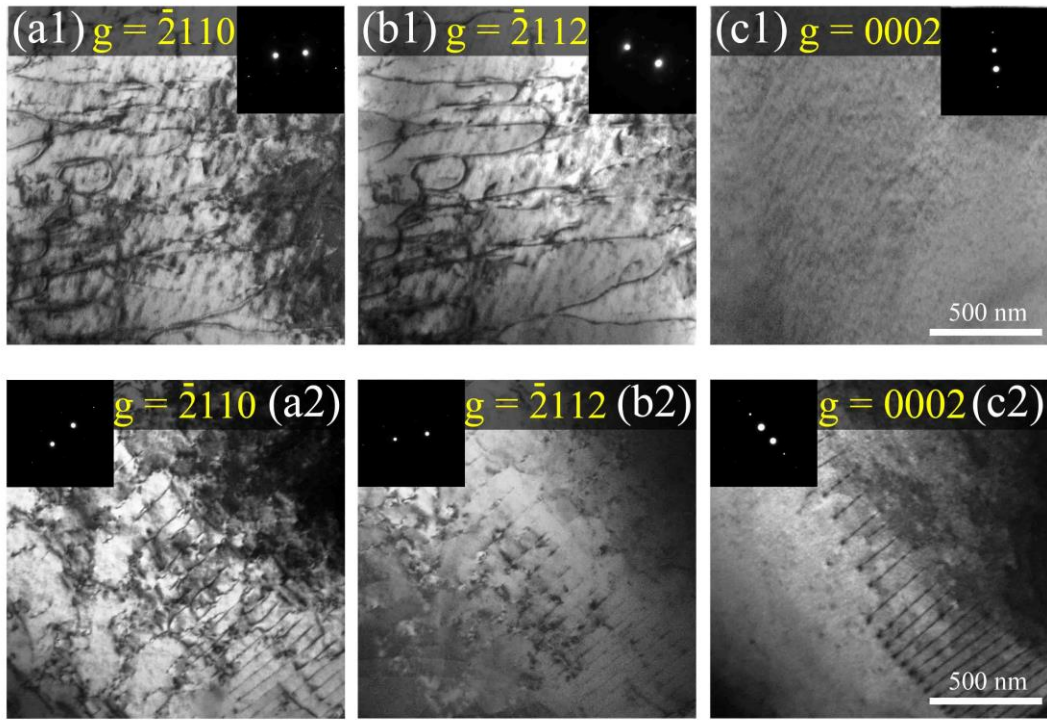


Fig. 5 TEM two-beam analysis at $\varepsilon_p=0.02$ with zone axis near $[01\bar{1}0]$ and diffraction vectors parallel to (a) $\bar{2}110$; (b) $\bar{2}112$, and (c) 0002 . The subfigures with level 1 correspond to Ti whereas those with level 2 correspond to Ti.2.

In summary, our novel strategy utilizes the high solute concentration and local fluctuations in MPEAs to boost $\langle c+a \rangle$ activity in HCP alloys. Applied to two Ti-Zr-Hf alloys, we showcase how these two core MPEA properties can synergize to enhance the $\text{Pyr1}\langle a \rangle$ and $\langle c+a \rangle$ activities, yielding a strength-toughness combination that outperforms all existing single-phase coarse-grained HCP materials. This strategy promises broad applicability to various MPEAs featuring an HCP structure. Further property improvements are anticipated through grain refinement, the introduction of hetero/hierarchical structures, or the application of precipitation and dislocation engineering, building upon their already impressive baseline reported here.

Acknowledgement

This work was supported by the National Natural Science Foundation of China (Nos. 52371119, 51801147, 51790482, 51722104, 51625103, and 51621063) and the

1 National Key Research and Development Program of China (No. 2017YFB0702301).
2
3 Drs. Ungár and Ribárik are acknowledged for sharing the CMWP code. Prof. Ruifeng
4 Zhang is acknowledged for sharing the PNADIS code. Besides, the authors would like
5
6 to express their gratitude to Dr. Máthis for his kind help with determining the
7
8 dislocation proportions, to Dr. Fuxue Yan and Wei Wang for their help with the electron
9
10 microscopes. Dr. Indranil Basu is acknowledged for fruitful discussion.
11
12
13
14
15

16 Reference

- 17
18 [1] Z. Wu, W.A. Curtin. Mechanism and energetics of $\langle c + a \rangle$ dislocation cross-slip in hcp metals, *Proc*
19 *Natl Acad Sci U S A* 113 (2016) 11137-11142.
20
21 [2] B.Y. Liu, F. Liu, N. Yang, X.B. Zhai, L. Zhang, Y. Yang, B. Li, J. Li, E. Ma, J.F. Nie, Z.W. Shan. Large
22 plasticity in magnesium mediated by pyramidal dislocations, *Science* 365 (2019) 73-75.
23
24 [3] T. Wang, M. Zha, C. Du, H.-L. Jia, C. Wang, K. Guan, Y. Gao, H.-Y. Wang. High strength and high
25 ductility achieved in a heterogeneous lamella-structured magnesium alloy, *Materials Research Letters*
26 11 (2022) 187-195.
27
28 [4] Q. Yu, Z.W. Shan, J. Li, X. Huang, L. Xiao, J. Sun, E. Ma. Strong crystal size effect on deformation
29 twinning, *Nature* 463 (2010) 335-338.
30
31 [5] S. Zhao, R. Zhang, Q. Yu, J. Ell, R.O. Ritchie, A.M. Minor. Cryoforged nanotwinned titanium with
32 ultrahigh strength and ductility, *Science* 373 (2021) 1363-1368.
33
34 [6] Y. Chong, M. Poschmann, R. Zhang, S. Zhao, M.S. Hooshmand, E. Rothchild, D.L. Olmsted, J. Morris
35 Jr, D.C. Chrzan, M. Asta. Mechanistic basis of oxygen sensitivity in titanium, *Science advances* 6 (2020)
36 eabc4060.
37
38 [7] T. Hama, A. Kobuki, H. Takuda. Crystal-plasticity finite-element analysis of anisotropic deformation
39 behavior in a commercially pure titanium Grade 1 sheet, *International Journal of Plasticity* 91 (2017) 77-
40 108.
41
42 [8] D. Li, G. Fan, X. Huang, D. Juul Jensen, K. Miao, C. Xu, L. Geng, Y. Zhang, T. Yu. Enhanced strength in
43 pure Ti via design of alternating coarse- and fine-grain layers, *Acta Materialia* 206 (2021) 116627.
44
45 [9] J. Koike, T. Kobayashi, T. Mukai, H. Watanabe, M. Suzuki, K. Maruyama, K. Higashi. The activity of
46 non-basal slip systems and dynamic recovery at room temperature in fine-grained AZ31B magnesium
47 alloys, *Acta Materialia* 51 (2003) 2055-2065.
48
49 [10] A. Fitzner, D.G.L. Prakash, J.Q. da Fonseca, M. Thomas, S.-Y. Zhang, J. Kelleher, P. Manuel, M. Preuss.
50 The effect of aluminium on twinning in binary alpha-titanium, *Acta Materialia* 103 (2016) 341-351.
51
52 [11] Y. Chong, R. Zhang, M.S. Hooshmand, S. Zhao, D.C. Chrzan, M. Asta, J.W. Morris, Jr., A.M. Minor.
53 Elimination of oxygen sensitivity in alpha-titanium by substitutional alloying with Al, *Nat Commun* 12
54 (2021) 6158.
55
56 [12] D. Truax, C. McMahon Jr. Plastic behavior of titanium-aluminum alloys, *Materials Science and*
57 *Engineering* 13 (1974) 125-139.
58
59 [13] S. Sandlobes, M. Friak, S. Korte-Kerzel, Z. Pei, J. Neugebauer, D. Raabe. A rare-earth free
60 magnesium alloy with improved intrinsic ductility, *Sci Rep* 7 (2017) 10458.
61
62
63
64
65

- 1 [14] C. Wang, H.-Y. Zhang, H.-Y. Wang, G.-J. Liu, Q.-C. Jiang. Effects of doping atoms on the generalized
2 stacking-fault energies of Mg alloys from first-principles calculations, *Scripta Materialia* 69 (2013) 445-
3 448.
- 4 [15] P. Kwasniak, H. Garbacz, K.J. Kurzydowski. Solid solution strengthening of hexagonal titanium
5 alloys: Restoring forces and stacking faults calculated from first principles, *Acta Materialia* 102 (2016)
6 304-314.
- 7 [16] D. Buey, L.G. Hector, M. Ghazisaeidi. Core structure and solute strengthening of second-order
8 pyramidal $\langle c+a \rangle$ dislocations in Mg-Y alloys, *Acta Materialia* 147 (2018) 1-9.
- 9 [17] N. Li, C. Wang, M.A. Monclús, L. Yang, J.M. Molina-Aldareguia. Solid solution and precipitation
10 strengthening effects in basal slip, extension twinning and pyramidal slip in Mg-Zn alloys, *Acta Materialia*
11 221 (2021) 117374.
- 12 [18] Z.R. Zeng, M.Z. Bian, S.W. Xu, C.H.J. Davies, N. Birbilis, J.F. Nie. Effects of dilute additions of Zn and
13 Ca on ductility of magnesium alloy sheet, *Materials Science and Engineering: A* 674 (2016) 459-471.
- 14 [19] Y. Bu, Z. Li, J. Liu, H. Wang, D. Raabe, W. Yang. Nonbasal Slip Systems Enable a Strong and Ductile
15 Hexagonal-Close-Packed High-Entropy Phase, *Phys Rev Lett* 122 (2019) 075502.
- 16 [20] Y. Ogawa, A. Singh, H. Somekawa. Activation of non-basal $\langle c+a \rangle$ slip in coarse-grained Mg-Sc alloy,
17 *Scripta Materialia* 218 (2022) 114830.
- 18 [21] S. Sandlöbes, M. Friák, S. Zaefferer, A. Dick, S. Yi, D. Letzig, Z. Pei, L.F. Zhu, J. Neugebauer, D. Raabe.
19 The relation between ductility and stacking fault energies in Mg and Mg-Y alloys, *Acta Materialia* 60
20 (2012) 3011-3021.
- 21 [22] S. Sandlöbes, Z. Pei, M. Friák, L.F. Zhu, F. Wang, S. Zaefferer, D. Raabe, J. Neugebauer. Ductility
22 improvement of Mg alloys by solid solution: Ab initio modeling, synthesis and mechanical properties,
23 *Acta Materialia* 70 (2014) 92-104.
- 24 [23] Z. Wu, W.A. Curtin. The origins of high hardening and low ductility in magnesium, *Nature* 526 (2015)
25 62-67.
- 26 [24] Z. Wu, R. Ahmad, B. Yin, S. Sandlöbes, W. Curtin. Mechanistic origin and prediction of enhanced
27 ductility in magnesium alloys, *Science* 359 (2018) 447-452.
- 28 [25] R. Pei, Y. Zou, D. Wei, T. Al-Samman. Grain boundary co-segregation in magnesium alloys with
29 multiple substitutional elements, *Acta Materialia* 208 (2021) 116749.
- 30 [26] C. Liu, H. Chen, J.-F. Nie. Interphase boundary segregation of Zn in Mg-Sn-Zn alloys, *Scripta*
31 *Materialia* 123 (2016) 5-8.
- 32 [27] J.F. Nie, Y.M. Zhu, J.Z. Liu, X.Y. Fang. Periodic segregation of solute atoms in fully coherent twin
33 boundaries, *Science* 340 (2013) 957-960.
- 34 [28] B. Raeisina, S.R. Agnew, A. Akhtar. Incorporation of Solid Solution Alloying Effects into Polycrystal
35 Modeling of Mg Alloys, *Metallurgical and Materials Transactions A* 42 (2010) 1418-1430.
- 36 [29] N. Stanford, M. Barnett. Solute strengthening of prismatic slip, basal slip and twinning in Mg and
37 Mg-Zn binary alloys, *International Journal of Plasticity* 47 (2013) 165-181.
- 38 [30] Z.N. Yang, X.B. Wang, F. Liu, F.C. Zhang, L.J. Chai, R.S. Qiu, L.Y. Chen. Effect of intercritical annealing
39 temperature on microstructure and mechanical properties of duplex Zr-2.5Nb alloy, *Journal of Alloys*
40 *and Compounds* 776 (2019) 242-249.
- 41 [31] M. Zhang, F. Zhang, Z. Yang, Y. Li, L. Qu, H. Zhen. Effect of cooling process on the formation of
42 duplex microstructure in Zr-2.3Nb alloy, *Journal of Alloys and Compounds* 651 (2015) 316-321.
- 43 [32] H. Yang, J. Shen, Y. Matsukawa, Y. Satoh, S. Kano, Z. Zhao, Y. Li, F. Li, H. Abe. Effects of alloying
44 elements (Sn, Nb, Cr, and Mo) on the microstructure and mechanical properties of zirconium alloys,
45
46
47
48
49
50
51
52
53
54
55
56
57
58
59
60
61
62
63
64
65

Journal of Nuclear Science and Technology 52 (2015) 1162-1173.

- 1 [33] S.H. Ahn, Y.B. Chun, S.H. Yu, K.H. Kim, S.K. Hwang. Microstructural refinement and deformation
2 mode of Ti under cryogenic channel die compression, *Materials Science and Engineering: A* 528 (2010)
3 165-171.
4
5 [34] B. Alobaid. Mechanical properties of cryo-rolled commercially pure titanium, *IOP Conference*
6 *Series: Materials Science and Engineering* 1090 (2021) 012115.
7
8 [35] B. Barkia, V. Doquet, J.P. Couzinié, I. Guillot, E. Héripré. In situ monitoring of the deformation
9 mechanisms in titanium with different oxygen contents, *Materials Science and Engineering: A* 636 (2015)
10 91-102.
11
12 [36] V.A. Moskalenko, A.R. Smirnov, Y.M. Plotnikova, I.S. Braude, R.V. Smolianets. Fundamentals of
13 titanium nanocrystalline structure creation by cryomechanical grain fragmentation, *Materials Science*
14 *and Engineering: A* 700 (2017) 707-713.
15
16 [37] V.V. Stolyarov, Y.T. Zhu, I.V. Alexandrov, T.C. Lowe, R.Z. Valiev. Influence of ECAP routes on the
17 microstructure and properties of pure Ti, *Materials Science and Engineering: A* 299 (2001) 59-67.
18
19 [38] J.W. Won, J.H. Lee, J.S. Jeong, S.-W. Choi, D.J. Lee, J.K. Hong, Y.-T. Hyun. High strength and ductility
20 of pure titanium via twin-structure control using cryogenic deformation, *Scripta Materialia* 178 (2020)
21 94-98.
22
23 [39] H. Wu, J. Jiang, H. Liu, J. Sun, Y. Gu, R. Tang, X. Zhao, A. Ma. Fabrication of an Ultra-Fine Grained
24 Pure Titanium with High Strength and Good Ductility via ECAP plus Cold Rolling, *Metals* 7 (2017) 563.
25
26 [40] X. Wu, M. Yang, F. Yuan, G. Wu, Y. Wei, X. Huang, Y. Zhu. Heterogeneous lamella structure unites
27 ultrafine-grain strength with coarse-grain ductility, *Proc Natl Acad Sci U S A* 112 (2015) 14501-14505.
28
29 [41] Y. Chong, M. Poschmann, R. Zhang, S. Zhao, M.S. Hooshmand, E. Rothchild, D.L. Olmsted, J. Morris,
30 D.C. Chrzan, M. Asta. Mechanistic basis of oxygen sensitivity in titanium, *Science advances* 6 (2020)
31 eabc4060.
32
33 [42] D.K. Yang, P.D. Hodgson, C.E. Wen. Simultaneously enhanced strength and ductility of titanium via
34 multimodal grain structure, *Scripta Materialia* 63 (2010) 941-944.
35
36 [43] S. Chen, D. Tubul, A. Venkert, D. Rittel. The Effect of Heat Treatment on the Mechanical Behavior
37 of Commercially Pure Titanium and Zirconium Under Quasi-static and Dynamic Loading, *Metallurgical*
38 *and Materials Transactions A* 53 (2022) 900-914.
39
40 [44] D.-s. Kang, K.-j. Lee, E.-p. Kwon, T. Tsuchiyama, S. Takaki. Variation of work hardening rate by oxygen
41 contents in pure titanium alloy, *Materials Science and Engineering: A* 632 (2015) 120-126.
42
43 [45] M. Wang, Y. Wang, Q. He, W. Wei, F. Guo, W. Su, C. Huang. A strong and ductile pure titanium,
44 *Materials Science and Engineering: A* 833 (2022) 142534.
45
46 [46] D. Guo, Z. Zhang, G. Zhang, M. Li, Y. Shi, T. Ma, X. Zhang. An extraordinary enhancement of strain
47 hardening in fine-grained zirconium, *Materials Science and Engineering: A* 591 (2014) 167-172.
48
49 [47] Z.N. Yang, Y.Y. Xiao, F.C. Zhang, Z.G. Yan. Effect of cold rolling on microstructure and mechanical
50 properties of pure Zr, *Materials Science and Engineering: A* 556 (2012) 728-733.
51
52 [48] C. Yuan, Y. Wang, D. Sang, Y. Li, L. Jing, R. Fu, X. Zhang. Effects of deep cryogenic treatment on the
53 microstructure and mechanical properties of commercial pure zirconium, *Journal of Alloys and*
54 *Compounds* 619 (2015) 513-519.
55
56 [49] X. Zhang, B. Zhang, S.G. Liu, C.Q. Xia, X.Y. Zhang, M.Z. Ma, R.P. Liu. Microstructures and mechanical
57 properties of Zr–Al binary alloys processed by hot-rolling, *Materials Science and Engineering: A* 773
58 (2020) 138723.
59
60 [50] R.S. Rajpurohit, N.C. Santhi Srinivas, S.R. Singh, V. Singh. Effect of Ratcheting on Tensile Behavior

of Zircaloy-2 at Room Temperature, Transactions of the Indian Institute of Metals 71 (2017) 1149-1160.

[51] K. Limbadri, S.K. Singh, K. Satyanarayana, A.K. Singh, A.M. Ram, M. Ravindran, K.V.M. Krishna, M.C. Reddy, K. Suresh. Orientation-Dependent Tensile Flow Behavior of Zircaloy-4 at Room Temperature, Metallography, Microstructure, and Analysis 7 (2018) 421-433.

[52] G. Singh, R. Verma, R. Jayaganthan. Influence of texture and microstructural evolution on ductility and tensile behaviour of annealed Zircaloy-4 processed through swaging, Journal of Materials Research and Technology 19 (2022) 4536-4542.

[53] D. Fuloria, N. Kumar, S. Goel, R. Jayaganthan, S. Jha, D. Srivastava. Tensile properties and microstructural evolution of Zircaloy-4 processed through rolling at different temperatures, Materials & Design 103 (2016) 40-51.

[54] J. Jiang, Y. Zhao, X. Wang. Effects of Zr addition on the deformation behavior, microstructure and mechanical properties of dental Ti alloys, Materials Science and Engineering: A 794 (2020) 139808.

[55] Y. Chong, T. Tsuru, B. Guo, R. Gholizadeh, K. Inoue, N. Tsuji. Ultrahigh yield strength and large uniform elongation achieved in ultrafine-grained titanium containing nitrogen, Acta Materialia 240 (2022) 118356.

[56] X. Liu, H. Gao, H. Wu, H. Pan, B. Shu, Y. Yang, H. Liu, F. Yang, X. Zhu. Microstructure and texture characteristics of pure Ti with a superior combination of strength and ductility, Materials Science and Engineering: A 808 (2021) 140915.

[57] J.W. Won, S.-W. Choi, J.-K. Hong, B.-C. Suh, J.H. Lee, B.J. Kwak. Microstructure and strength–ductility balance of pure titanium processed by cryogenic rolling at various rolling reductions, Materials Science and Engineering: A 798 (2020) 140328.

[58] H. Shi, J. Li, J. Mao, W. Lu. The elimination of the yield point phenomenon in a new zirconium alloy: Influence of degree of recrystallization on the tensile properties, Scripta Materialia 169 (2019) 28-32.

[59] S. Deng, H. Song, H. Liu, S.-H. Zhang. Effect of uniaxial loading direction on mechanical responses and texture evolution in cold pilgered Zircaloy-4 tube: Experiments and modeling, International Journal of Solids and Structures 213 (2021) 63-76.

[60] F. Han, G. Li, C. Liu, F. Yuan, Y. Zhang, M. Ali, W. Guo, H. Gu. Anisotropic yielding behavior and associated mechanism of cold rolled and annealed Zircaloy-4 alloy thin sheets under tensile condition, Materials Chemistry and Physics 242 (2020) 122539.

[61] W. Guo, G. Li, F. Yuan, F. Han, Y. Zhang, M. Ali, J. Ren, G. Yuan. Texture development and mechanical behavior of Zircaloy-4 alloy plates fabricated by cold rolling and annealing, Materials Science and Engineering: A 807 (2021) 140846.

[62] J.W. Zhang, I.J. Beyerlein, W.Z. Han. Hierarchical 3D Nanolayered Duplex-Phase Zr with High Strength, Strain Hardening, and Ductility, Phys Rev Lett 122 (2019) 255501.

[63] C. Yuan, R. Fu, D. Sang, Y. Yao, X. Zhang. The tensile properties and fracture behavior of gradient nano-grained/coarse-grained zirconium, Materials Letters 107 (2013) 134-137.

[64] J. Kuang, X. Du, X. Li, Y. Yang, A.A. Luo, G. Tang. Athermal influence of pulsed electric current on the twinning behavior of Mg–3Al–1Zn alloy during rolling, Scripta Materialia 114 (2016) 151-155.

[65] J. Kuang, T.S.E. Low, S.R. Niezgodá, X. Li, Y. Geng, A.A. Luo, G. Tang. Abnormal texture development in magnesium alloy Mg–3Al–1Zn during large strain electroplastic rolling: Effect of pulsed electric current, International Journal of Plasticity 87 (2016) 86-99.

[66] W. Wen, M. Borodachenkova, C.N. Tomé, G. Vincze, E.F. Rauch, F. Barlat, J.J. Grácio. Mechanical behavior of Mg subjected to strain path changes: Experiments and modeling, International Journal of Plasticity 73 (2015) 171-183.

- 1 [67] T. Ungár, O. Castelnau, G. Ribárik, M. Drakopoulos, J.L. Béchade, T. Chauveau, A. Snigirev, I.
2 Snigireva, C. Schroer, B. Bacroix. Grain to grain slip activity in plastically deformed Zr determined by X-
3 ray micro-diffraction line profile analysis, *Acta Materialia* 55 (2007) 1117-1127.
- 4 [68] M. Wang, X.Y. Xu, H.Y. Wang, L.H. He, M.X. Huang. Evolution of dislocation and twin densities in a
5 Mg alloy at quasi-static and high strain rates, *Acta Materialia* 201 (2020) 102-113.
- 6 [69] D. Hull, D.J. Bacon. Introduction to dislocations, Elsevier, 2011.
- 7 [70] H. Van Swygenhoven, P.M. Derlet, A.G. Frøseth. Stacking fault energies and slip in nanocrystalline
8 metals, *Nature Materials* 3 (2004) 399-403.
- 9 [71] G. Lu, N. Kioussis, V.V. Bulatov, E. Kaxiras. Generalized-stacking-fault energy surface and dislocation
10 properties of aluminum, *Phys. Rev. B* 62 (2000) 3099-3108.
- 11 [72] S.H. Zhang, D. Legut, R.F. Zhang. PNADIS: An automated Peierls–Nabarro analyzer for dislocation
12 core structure and slip resistance, *Computer Physics Communications* 240 (2019) 60-73.
- 13 [73] Q.J. Li, H. Sheng, E. Ma. Strengthening in multi-principal element alloys with local-chemical-order
14 roughened dislocation pathways, *Nat Commun* 10 (2019) 3563.
- 15 [74] S. Lee, M.J. Duarte, M. Feuerbacher, R. Soler, C. Kirchlechner, C.H. Liebscher, S.H. Oh, G. Dehm.
16 Dislocation plasticity in FeCoCrMnNi high-entropy alloy: quantitative insights from in situ transmission
17 electron microscopy deformation, *Materials Research Letters* 8 (2020) 216-224.
- 18 [75] C. Kale, P. Garg, B.G. Bazehour, S. Srinivasan, M.A. Bhatia, P. Peralta, K.N. Solanki. Oxygen effects
19 on crystal plasticity of Titanium: A multiscale calibration and validation framework, *Acta Materialia* 176
20 (2019) 19-32.
- 21 [76] S.R. Agnew, L. Capolungo, C.A. Calhoun. Connections between the basal l_1 “growth” fault and
22 $\langle c+a \rangle$ dislocations, *Acta Materialia* 82 (2015) 255-265.
- 23 [77] I. Basu, M. Chen, J. Wheeler, R.E. Schäublin, J.F. Löffler. Segregation-driven exceptional twin-
24 boundary strengthening in lean Mg–Zn–Ca alloys, *Acta Materialia* 229 (2022) 117746.
- 25 [78] Y. Tang, J.A. El-Awady. Formation and slip of pyramidal dislocations in hexagonal close-packed
26 magnesium single crystals, *Acta Materialia* 71 (2014) 319-332.
- 27 [79] C. He, Y. Zhang, C.Q. Liu, Y. Yue, H.W. Chen, J.F. Nie. Unexpected partial dislocations within stacking
28 faults in a cold deformed Mg–Bi alloy, *Acta Materialia* 188 (2020) 328-343.
- 29 [80] C. Niu, C.R. LaRosa, J. Miao, M.J. Mills, M. Ghazisaeidi. Magnetically-driven phase transformation
30 strengthening in high entropy alloys, *Nat Commun* 9 (2018) 1363.
- 31 [81] Z. Li, K.G. Pradeep, Y. Deng, D. Raabe, C.C. Tasan. Metastable high-entropy dual-phase alloys
32 overcome the strength-ductility trade-off, *Nature* 534 (2016) 227-230.
- 33 [82] M. Naeem, H. He, F. Zhang, H. Huang, S. Harjo, T. Kawasaki, B. Wang, S. Lan, Z. Wu, F. Wang.
34 Cooperative deformation in high-entropy alloys at ultralow temperatures, *Science Advances* 6 (2020)
35 eaax4002.
- 36 [83] D.D. Zhang, J.Y. Zhang, J. Kuang, G. Liu, J. Sun. Superior strength-ductility synergy and strain
37 hardenability of Al/Ta co-doped NiCoCr twinned medium entropy alloy for cryogenic applications, *Acta*
38 *Materialia* 220 (2021) 117288.
- 39 [84] R.C. Picu. A mechanism for the negative strain-rate sensitivity of dilute solid solutions, *Acta*
40 *Materialia* 52 (2004) 3447-3458.
- 41 [85] Y. Chong, R. Gholizadeh, T. Tsuru, R. Zhang, K. Inoue, W. Gao, A. Godfrey, M. Mitsuhashi, J.W. Morris,
42 Jr., A.M. Minor, N. Tsuji. Grain refinement in titanium prevents low temperature oxygen embrittlement,
43 *Nat Commun* 14 (2023) 404.
- 44
45
46
47
48
49
50
51
52
53
54
55
56
57
58
59
60
61
62
63
64
65



[Click here to access/download](#)

Supplementary Material

Supplementary Materials_TiZrHf_V1.4.docx



Declaration of interests

The authors declare that they have no known competing financial interests or personal relationships that could have appeared to influence the work reported in this paper.

The authors declare the following financial interests/personal relationships which may be considered as potential competing interests: